Extensive spatio-temporal analyses of surface ozone and related meteorological variables in South Korea for 1999–2010

Jihoon Seo,[1,3] Daeok Youn,[2*] Jin Young Kim,[1] and Huikyo Lee[4]

[1]Green City Technology Institute, Korea Institute of Science and Technology, Seoul, South Korea

[2]Department of Earth Science Education, Chungbuk National University, Cheongju, South Korea

[3]School of Earth and Environmental Sciences, Seoul National University, Seoul, South Korea

[4]Jet Propulsion Laboratory, California Institute of Technology, Pasadena, CA, USA

April 25, 2014

[*]Corresponding author:

Daeok Youn

Department of Earth Science Education

Chungbuk National University, Cheongju, South Korea

Tel: +82-43-261-2738

E-mail: dyoun@chungbuk.ac.kr

Abstract

Spatio-temporal characteristics of surface ozone (O_3) variations over South Korea are investigated with consideration of meteorological factors and time scales based on the Kolmogorov-Zurbenko filter (KZ-filter), using measurement data at 124 air quality monitoring sites and 72 weather stations for the 12-yr period of 1999–2010. In general, O_3 levels at coastal cities are high due to dynamic effects of the sea breeze while those at the inland and Seoul Metropolitan Area (SMA) cities are low due to the NO_x titration by local precursor emissions. We examine the meteorological influences on O_3 using a combined analysis of the KZ-filter and linear regressions between O_3 and meteorological variables. We decomposed O_3 time series at each site into short-term, seasonal, and long-term components by the KZ-filter and regressed on meteorological variables. Impact of temperature on the O_3 levels is significantly high in the highly populated SMA and inland region, but low in the coastal region. In particular, the probability of high O_3 occurrence doubles with 4°C of temperature increase in the SMA during high O_3 months (May to October). This implies that those regions will experience frequent high O_3 events in a future warming climate. In terms of short-term variation, the distribution of high O_3 probability classified by wind direction shows the effect of both local precursor emissions and long-range transport from China. In terms of long-term variation, the O_3 concentrations have increased by +0.26 ppbv yr^{-1} on nationwide average, but their trends show large spatial variability. Singular value decomposition analyses further reveal that the long-term temporal evolution of O_3 is similar to that of nitrogen dioxide, although the spatial distribution of their trends is different. This study will be helpful as a reference for diagnostics and evaluation of regional- and local-scale O_3 and climate simulations, and as a guide to appropriate O_3 control policy in South Korea.

Keywords: South Korea, surface ozone, KZ-filter, temporal trends, meteorological effects

1. Introduction

Surface ozone (O_3) is a well-known secondary air pollutant, which affects air quality, human health, and vegetation. High O_3 concentration has detrimental effects on respiration, lung function, and airway reactivity in human health (Bernard et al., 2001; Bell et al., 2007). In terms of mortality, Levy et al. (2005) has previously assessed that 10 ppbv increase in 1-h maximum O_3 could increase daily mortality by 0.41%. High O_3 concentrations could also reduce agricultural production. For example, Wang and Mauzerall (2004) reported that the East Asian countries of China, Japan, and South Korea lost 1–9% of their yields of wheat, rice, and corn, and 23–27% of their yields of soybeans due to O_3 in 1990. In addition, O_3 is one of greenhouse gases of which radiative forcing is estimated as the third largest contribution among the various constituents in the troposphere (IPCC, 2007). Therefore, the spatially inhomogeneous distribution of O_3 due to its short chemical lifetime of a week to a month could induce strong regional-scale climate responses (Mickley et al., 2004).

In the Northern Hemisphere mid-latitudes where population, industry, and transportation are concentrated, the background O_3 levels increased during the late 20th century due to increases in anthropogenic precursors particularly nitrogen oxides (NO_x), but its trends show regional and temporal differences (Oltmans et al., 1998; Guicherit and Roemer, 2000; Vingarzan, 2004). Although the increasing trends of O_3 in Europe, North Atlantic, North America, and Japan have flattened over the past decade (Oltmans et al., 2006; Oltmans et al., 2013), there have still been concerns about elevated O_3 concentration in China owing to rapid economic growth and industrialization (Ding et al., 2008; Tang et al., 2009; Wang et al., 2009; Wang et al., 2012). Such recent increases of O_3 in China can affect the regional background O_3 levels in East Asia by transboundary transport of O_3 and its precursors. For example, previous modeling studies have shown that the transport of O_3 from China by continental outflow is one of the major contributions of O_3 in Japan and South Korea (Tanimoto et al., 2005; Nagashima et al., 2010). Intercontinental transport of O_3 and its precursors originated from East Asia affects O_3 concentrations and air quality in remote areas even on a global scale (Akimoto, 2003). Experiments using a global climate-chemistry model with future emission scenarios by Lei et al. (2013) suggest that the increase in East Asian emissions will still be an important issue for the O_3 air quality in both East Asia and United States.

Recently, several studies have focused on the relationship between O_3 levels and temperature, and suggested potential influences of the global warming and climate change

on the high levels of O_3 (Jacob and Winner, 2009; Rasmussen et al., 2012; and references therein). Lin et al. (2001) calculated probability of daily maximum 8-h average O_3 exceeding 85 ppbv for a given range of daily maximum temperatures and reported that a 3°C increase of the daily maximum temperature doubles risk of O_3 exceedances in the Northeastern United States. In addition, Ordóñez et al. (2005) showed that high temperature extremes probably led to the high occurrence of severe O_3 episodes during the summer 2003 heat wave over Europe. These results imply the potentially large sensitivity of O_3 concentration and related air quality to the temperature increases (Jacob and Winner, 2009). In the model experiments by Lin et al. (2008), both averaged O_3 concentration and frequencies of high O_3 episodes were predicted to increase in the future over the United States and East Asia. Recent global climate-chemistry model experiments by Lei and Wang (2014) also implied the future O_3 increases in industrial regions due to more O_3 productions by photochemical reactions and less O_3 removals by nocturnal odd nitrogen (NO_y) chemistry in warmer condition.

In South Korea, one of the most highly populated countries in the world, both O_3 concentration and high O_3 episodes have increased in recent decades despite efforts to regulate emissions of O_3 precursors (KMOE, 2012). Although the increase of O_3 levels in South Korea over the last three decades is mainly regarded as the results of rapid industrialization, economic expansion, and urbanization, there are other factors to be considered to explain the long-term increase in O_3 concentration. For example, since the Korean peninsula is located on the eastern boundary of East Asia, downward transport of O_3 by the continental outflow considerably affects the high O_3 levels in South Korea (Oh et al., 2010). In addition, recent warming trend related to global climate change could also be an important factor to increase O_3 concentration in South Korea. Climate change is expected to increase both frequency and intensity of temperature extremes over the Korean peninsula (Boo et al., 2006). Therefore, comprehensive understanding of the various factors affecting O_3 concentration, such as local precursor emissions, transport of O_3 and its precursors from local and remote sources, and changes in meteorological fields related to climate change is required to guide environmental policies.

The present study aims to examine the spatio-temporal characteristics of the measured O_3 variations in South Korea with consideration of three time scales and various meteorological factors, using ground-measured data from 124 air quality monitoring sites and 72 weather stations for the 12-yr period of 1999–2010. We decomposed O_3 time series at each measurement site into different time scale of short-term, seasonal, and long-term

components by application of the Kolmogorov-Zurbenko filter (KZ-filter) that has been used in previous studies (e.g. Gardner and Dorling, 2000; Ibarra-Berastegi et al., 2001; Thompson et al., 2001; Lu and Chang, 2005; Wise and Comrie, 2005; Tsakiri and Zurbenko, 2011; Shin et al., 2012). To investigate the meteorological impact on the O_3 levels, we applied the combined analysis of the KZ-filter and linear regression model with the meteorological variables. In the short-term time scale, the possible effects of transport from the local and remote sources on the high O_3 episodes were explored by using the wind data. In the long-term time scale, the singular value decomposition (SVD) with nitrogen dioxide (NO_2) measurements was additionally applied to examine the effects of varying local emissions on the long-term O_3 trend.

The remainder of this paper is structured as follows. In the next section, we describe the observational data and analysis techniques used in this study. In Sect. 3, we investigated the spatio-temporal characteristics of the decomposed O_3 time series and its relationship with meteorological variables over South Korea. Finally, the key findings are summarized in Sect. 4.

2. Data and methodologies

2.1. Data

The National Institute of Environmental Research (NIER) of South Korea provides hourly data of O_3 and NO_2 mixing ratios in the ppbv unit, which have been measured by ultraviolet absorption and chemiluminescence respectively. We here select 124 urban air quality monitoring sites over South Korea, based on data availability for the period 1999–2010, and analyze hourly time series of O_3 and NO_2 from each site. It is noted that our current analysis exclude other data from roadside measurement sites where data can be directly affected by the vehicle exhaust emissions and suburban and background sites located around South Korea. Hourly meteorological data at 72 weather stations of the Korea Meteorological Administration (KMA) for the same period are also used to examine the effects of meteorological factors on the O_3 variations. The meteorological variables used in this study include common factors related to the O_3 variations such as temperature (°C), surface insolation (W m^{-2}), relative humidity (%), and wind speed (m s^{-1}) (e.g. Ordóñez et al., 2005; Camalier et al., 2007; Jacob and Winner, 2009). Dew-point temperature (°C) and sea-level pressure (hPa) are additionally applied for multiple linear regression models as other previous studies have done (e.g., Thompson et al., 2001; Shin et al., 2012). Finally wind direction (16 cardinal directions) is used to reveal its

relationship with short-term changes in O_3. Using the hourly data, we first calculated daily averages for O_3 ($O_{3\,avg}$), NO_2 ($NO_{2\,avg}$), temperature (T), surface insolation (SI), dew-point temperature (TD), sea-level pressure (PS), wind speed (WS), wind direction (WD), and relative humidity (RH). We also obtained daily minimum O_3 ($O_{3\,min}$), daily maximum 8-h average O_3 ($O_{3\,8h}$), and daily maximum temperature (T_{max}) from the hourly data set.

To investigate the relationship between O_3 and meteorological variables, it is desirable to use data observed at the same stations. However, not all of air quality monitoring sites and weather stations are closely located in South Korea. Therefore, we assume that an air quality monitoring site can observe the same meteorological variables as those at a weather station if the distance between the two places is less than 10 km. Under the assumption, only O_3 data from 72 air quality monitoring sites and meteorological data from 25 weather stations are available to analyze the meteorological effects on the O_3 variation over South Korea. The insolation was measured only at 17 weather stations for the analysis period. Figure 1 shows geographical locations of the ground measurements used in the present study, together with colored topography based on the U.S. Geological Survey (USGS) Digital Elevation Model (DEM).

2.2. Decomposition of O_3 time series by KZ-filter

The KZ-filter is a decomposition method than can be used to separate time series into short-term, seasonal, and long-term components (Rao and Zurbenko, 1994). We applied the KZ-filter to the O_3 time series by taking moving average of window length m with iterating p times, which is denoted by $KZ_{m,p}$. The KZ-filter is basically low-pass filter for removing high frequency components from the original time series. Following Eskridge et al. (1997), the KZ-filter removes the signal smaller than the period N, which is called as the effective filter width. N is defined as follows:

$$m \times p^{1/2} \le N \quad (1)$$

The KZ-filter method has the same level of accuracy as the wavelet transform method although it is much easier way to decompose the original time series (Eskridge et al., 1997). In addition, time series with missing observations can be applicable to KZ-filter owing to the iterative moving average process.

For the clear separation of the components, we applied KZ-filter to the daily log-transformed O_3 as in Rao and Zurbenko (1994) and Eskridge et al. (1997), instead of the raw O_3 concentrations. While the short-term component separated by the KZ-filter using

raw O_3 data still shows clear seasonality, use of $ln(O_3)$ makes the short-term component stationary and nearly independent of the seasonal influence by stabilizing variance (Rao and Zurbenko, 1994; Rao et al., 1997). Note that a temporal linear trend of log-transformed data is provided as % yr^{-1} because the differential of the natural logarithm is equivalent to the percentage change.

The natural logarithm of the O_3 time series at each site denoted as $[O_3](t)$ is thus decomposed by KZ-filter as follows:

$$[O_3](t) = [O_{3\,ST}](t) + [O_{3\,SEASON}](t) + [O_{3\,LT}](t) \quad (2)$$

$[O_{3\,ST}]$ is a short-term component attributable to day-to-day variation of synoptic-scale weather and short-term fluctuation in precursor emissions. $[O_{3\,SEASON}]$ represents a seasonal component related to the seasonal changes in solar radiation and vertical transport of O_3 from the stratosphere whose time scale is from several weeks to months. $[O_{3\,LT}]$ denotes a long-term component explained by changes in precursor emission, transport, climate, policy, and economy over the entire period (Rao et al., 1997; Milanchus et al., 1998; Gardner and Dorling, 2000; Thompson et al., 2001; Wise and Comrie, 2005). Tsakiri and Zurbenko (2011) showed that $[O_{3\,ST}]$ and $[O_{3\,LT}]$ are independent of each other. Also, statistical characteristics of $[O_{3\,ST}]$ are very close to those of white noise (Flaum et al., 1996) and therefore, $[O_{3\,ST}]$ is nearly detrended.

In this study, we used the KZ-filter with the window length of 29 days and 3 iterations ($KZ_{29,3}$) following previous studies (e.g., Rao and Zurbenko, 1994) and decomposed daily $ln(O_{3\,8h})$ time series at the 124 monitoring sites. $KZ_{29,3}$ removes $[O_{3\,ST}]$ of which the period is smaller than about 50 days, following Eq. (1). We defined the filtered time series as a baseline ($[O_{3\,BL}]$) as in Eq. (3).

$$[O_3](t) = [O_{3\,BL}](t) + [O_{3\,ST}](t) \quad (3)$$

Eq. (3) accounts for the multiplicative effects of short-term fluctuations on the $[O_{3\,BL}]$ due to the log-transformation (Thompson et al., 2001). In other words, exponential of $[O_{3\,ST}]$ is a ratio of the raw O_3 concentrations to the exponential of $[O_{3\,BL}]$, which is the baseline O_3 concentration in ppbv. Therefore, if $\exp[O_{3\,ST}]$ is larger than 1, the raw O_3 concentration will be larger than the baseline O_3 concentration.

$[O_{3\,BL}]$ is expressed as the sum of $[O_{3\,SEASON}]$ and $[O_{3\,LT}]$, as in Eq. (4) (Milanchus et al., 1998).

$$[O_{3\,BL}](t) = [O_{3\,SEASON}](t) + [O_{3\,LT}](t) \quad (4)$$

Since $[O_{3\,BL}]$ is closely associated with meteorological fields, we built a multiple regression model with available meteorological variables as in Eq. (5), following previous studies (e.g., Rao and Zurbenko, 1994; Rao et al., 1995; Ibarra-Berastegi et al., 2001). Short-term variability of meteorological variables was also filtered out by $KZ_{29,3}$.

$$[O_{3\,BL}](t) = a_0 + \sum_i a_i \mathrm{MET}_{BL}(t)_i + \varepsilon(t)$$
$$\mathrm{MET}_{BL}(t) = \left[T_{\max BL}(t), \mathrm{SI}_{BL}(t), \mathrm{TD}_{BL}(t), \mathrm{PS}_{BL}(t), \mathrm{WS}_{BL}(t), \mathrm{RH}_{BL}(t)\right] \quad (5)$$

In the multiple linear regression model, $[O_{3\,BL}]$ is a response variable and the baselines of meteorological variables ($\mathrm{MET}_{BL}(t)_i$) are predictors. Also, a_0, a_i, and $\varepsilon(t)$ denote the constant, regression coefficient of variable i, and residual of the multiple regression model, respectively.

The residual term $\varepsilon(t)$ contains not only the long-term variability of O_3 related to long-term changes in local precursor emissions but also seasonal variability of O_3 attributable to unconsidered meteorological factors in the multiple linear regression model. Thus, we applied the KZ-filter with the window length of 365 days and 3 iterations ($KZ_{365,3}$) to $\varepsilon(t)$ to extract the meteorologically adjusted $[O_{3\,LT}]$ of which the period is larger than about 1.7 yr as follow:

$$\varepsilon(t) = \mathrm{KZ}_{365,3}\left[\varepsilon(t)\right] + \delta(t) = [O_{3\,LT}](t) + \delta(t) \quad (6)$$

In Eq. (6), $\delta(t)$ denotes the seasonal variability of O_3 related to the meteorological variables unconsidered in the multiple linear regression model and/or noise.

Finally, $[O_{3\,SEASON}]$ is obtained by sum of the combined meteorological variables regressed on $[O_{3\,BL}]$ ($a_0 + \sum_i a_i\, \mathrm{MET}_{BL}(t)_i$) and $\delta(t)$ as in Eq. (7).

$$[O_{3\,SEASON}](t) = a_0 + \sum_i a_i \mathrm{MET}_{BL}(t)_i + \delta(t) \quad (7)$$

Figure 2 shows a schematic representation of Eq. (2) using daily $O_{3\,8h}$ time series at the City Hall of Seoul for the period of 1999–2010. $[O_{3\,SEASON}]$ in Fig. 2c clearly shows the typical seasonal cycle of O_3 in South Korea with high concentrations in spring, slight decrease in July and August, and increase in autumn (Ghim and Chang, 2000). The spring maximum of O_3 concentration in the Northern Hemisphere is generally attributed to episodic stratospheric intrusion (Levy et al., 1985; Logan, 1985), photochemical reactions of accumulated NO_x and hydrocarbons during the winter (Dibb et al., 2003), accumulation of O_3 due to the longer photochemical lifetime (~200 days) during the winter (Liu et al., 1987), and transport of O_3 and its precursors by the continental outflow (Carmichael et al., 1998; Jacob et al., 1999; Jaffe et al., 2003). On the other hand, frequent precipitation

during the East Asian summer monsoon influences the decrease of O_3 concentrations in July and August (Ghim and Chang, 2000). [$O_{3\ LT}$] in Fig. 2d shows that the O_3 concentrations at the monitoring site have increased in the past decade, irrespective of any change in meteorological conditions. It should be noted that [$O_{3\ LT}$] explains only 1.7% of the total variance of [O_3] at this site as its small ranges in Fig. 2d, while relative contributions of [$O_{3\ ST}$] and [$O_{3\ SEASON}$] are 58.3% and 32.7%, respectively. Therefore, the long-term changes in O_3 related to changes in local emission occupy only small fraction of the O_3 variations. The relative contributions of each component are further examined in Sect. 3.4.

2.3. Spatial interpolation by AIDW method

The inverse-distance weighting (IDW) is a deterministic spatial interpolation technique for spatial mapping of variables distributed at irregular points. In this study, we adopted the enhanced version of the IDW, the adaptive inverse-distance weighting (AIDW) technique (Lu and Wong, 2008). While the traditional IDW uses a fixed distance-decay parameter without considering the distribution of data within it, the AIDW uses adjusted distance-decay parameters according to density of local sampling points. Therefore, the AIDW provides flexibility to accommodate variability in the distance-decay relationship over the domain and thus better spatial mapping of variables distributed at irregular observational points (Lu and Wong, 2008).

In the mapping of O_3 with spatial interpolation, there are ubiquitous problems such as spatial-scale violations, improper evaluations, inaccuracy, and inappropriate use of O_3 maps in certain analyses (Diem, 2003). The spatial mapping in the present study also has problems with the spatial resolution of the observation, which is not high enough to consider small-scale chemical processes and geographical complexity of the Korean peninsula (see Fig. 1). Most of the air quality monitoring sites are concentrated on the cities, and typical inter-city distances are 30–100 km in South Korea while spatial representativeness of O_3 concentration is possibly as small as around 3–4 km (Tilmes and Zimmermann, 1998) or 5 km (Diem, 2003). In addition, mapping with a few monitoring sites combined with complex mountainous terrain can also distort the actual distribution of data, especially in the northeastern part of South Korea. Despite such limits, the spatial mapping in this study is still useful because we aim not to derive an exact value at a specific point where the observation does not exist, but to provide the better quantitative

understanding of O_3 and related factors in South Korea, especially focused on the metropolitan and urban areas.

3. Results

3.1. Spatial characteristics of O_3 and its trend in South Korea

Climatological daily average O_3 ($O_{3\ avg}$) and its temporal linear trends are represented in Fig. 3 and Table 1 using data from 124 monitoring sites distributed nationwide in 46 cities for the past 12-yr period. The spatial map of climatological daily average NO_2 ($NO_{2\ avg}$) is also shown in Fig. 3. In Table 1, the cities are categorized into three geographical groups: 16 coastal cities, 14 inland cities, and 16 cities in the Seoul Metropolitan Area (SMA). We separated the SMA cities from the other two groups since the SMA is the largest source region of anthropogenic O_3 precursors in South Korea. The SMA occupies only 11.8% (11,745 km^2) of the national area, but has 49% (25.4 million) of the total population and 45% (8.1 million) of total vehicles in South Korea. It is estimated that approximately 27% (0.29 Mt) of total NO_x emissions and 34% (0.30 Mt) of the volatile organic compounds (VOCs) emissions in South Korea are from the SMA in 2010 (KMOE, 2013). Therefore, the climatological $NO_{2\ avg}$ concentration in the SMA is much higher than that in other region (Fig. 3b).

In general, O_3 concentrations are high at the coastal cities, low at the inland cities, and lowest at the SMA cities in South Korea. Along with Table 1, Fig. 3a shows that the 12-yr average of $O_{3\ avg}$ is high at the southern coastal cities such as Jinhae (31.3 ppbv), Mokpo (30.3 ppbv), and Yeosu (28.1 ppbv), with the highest value at Jeju (32.6 ppbv), and low at the inland metropolitan cities such as Daegu (19.8 ppbv), Gwangju (20.5 ppbv), and Daejeon (20.7 ppbv), with lowest values at the SMA cities including Seoul (17.1 ppbv), Incheon (19.0 ppbv) and Anyang (16.8 ppbv).

Compared to the regional background concentration of 35–45 ppbv at five background measurement sites around South Korea (KMOE, 2012), the averaged O_3 concentrations in the SMA and inland metropolitans are much lower while those at the coastal cities are close to the regional background levels. In comparison with Fig. 3b, Fig. 3a shows that relatively lower $O_{3\ avg}$ regions are well consistent with relatively higher $NO_{2\ avg}$ regions. Substantial emissions of anthropogenic NO in the SMA and other inland metropolitans lead to NO_x titration effects even in the absence of photochemical reactions during the night, and thus the averaged O_3 concentrations are depressed by 10–20 ppbv lower than the regional background concentration (Ghim and Chang, 2000). A recent

293 modeling study by Jin et al. (2012) has suggested that the maximum O_3 concentrations in
294 the SMA, especially in Seoul and Incheon, are VOCs-limited. In the coastal region, on the
295 other hand, low emissions of NO with dilution by the strong winds weaken the titration
296 effect and result in the high O_3 concentrations. The dynamic effect of land-sea breeze is
297 another possible factor of the high O_3 levels at the coastal cities. Oh et al. (2006) showed
298 that a near-stagnant wind condition at the development of sea breeze temporarily contains
299 O_3 precursors carried by the offshore land breeze during the night, and following
300 photochemical reactions at mid-day produces O_3. The relationship between O_3 and wind
301 speed and direction will be shown in Sects. 3.2 and 3.5 respectively.
302 In terms of temporal trends, the surface O_3 concentrations in South Korea have
303 generally increased for the past 12 yr as shown in Fig. 3c and Table 1. The averaged
304 temporal linear trend of $O_{3\ avg}$ at 46 cities nationwide is +1.15% yr^{-1} (+0.26 ppbv yr^{-1}),
305 which is comparable with observed increasing trends of approximately +0.5–2% yr^{-1} in
306 various regions in the Northern Hemisphere (Vingarzan, 2004). Compared with previous
307 studies in East Asia, the overall increasing trend of O_3 in South Korea is smaller than
308 recent increasing trends over China of +1.1 ppbv yr^{-1} in Beijing for 2001–2006 (Tang et al.,
309 2009) and +0.58 ppbv yr^{-1} in Hong Kong for 1994–2007 (Wang et al., 2009) but slightly
310 larger than increasing trend over Japanese populated areas of +0.18 ppbv yr^{-1} for 1996–
311 2005 (Chatani and Sudo, 2011).
312 Several factors that could influence the overall increase of O_3 over East Asia were
313 suggested by the following previous studies. Recently, Zhao et al. (2013) have estimated
314 that the NO_x emissions in China increased rapidly from 11.0 Mt in 1995 to 26.1 Mt in
315 2010, mainly due to the fast growth of energy consumption. The NO_x and VOCs emissions
316 in South Korea also increased in the early 2000s. The estimated anthropogenic NOx and
317 VOCs emissions are 1.10 Mt and 0.74 Mt in 1999 but 1.35 Mt and 0.87 Mt in 2006,
318 respectively (KMOE, 2013). Tanimoto et al. (2009) suggested that the O_3 increase results
319 from such recently increased anthropogenic precursor emissions in East Asia.
320 However, model sensitivity simulations in Chatani and Sudo (2011) indicate that
321 the changes in East Asian emissions can explain only 30% of the O_3 trend. They have
322 suggested the long-term variations in meteorological fields as a possible important factor
323 although further studies are required. In particular, it is well known that insolation and
324 temperature are important meteorological factors in O_3 variation. While insolation directly
325 affects O_3 production through photochemical reactions, increased temperature affects net
326 O_3 production rather indirectly by increasing biogenic hydrocarbon emissions, hydroxyl

radical (OH) with more evaporation, and NO_x and HO_x radicals by thermal decomposition of peroxyacetyl nitrate (PAN) reservoir (Sillman and Samson, 1995; Olszyna et al., 1997; Racherla and Adams, 2006; Dawson et al., 2007). Therefore, the O_3 increasing trend in Fig. 3c is possibly affected by changes in meteorological variables.

Figure 4 shows temporal linear trends of daily average temperature (T) and insolation (SI). Despite the spatial discrepancy between trends of O_3 (Fig. 3c) and meteorological variables (Fig. 4), both temperature and insolation have generally increased in South Korea for the past 12 yr. The spatial mean of temporal linear trend in temperature at 72 weather stations nationwide is approximately +0.09°C yr^{-1}, which is much higher than +0.03°C yr^{-1} for the Northern Hemispheric land surface air temperature for 1979–2005 (IPCC, 2007). This high increasing trend of temperature in South Korea is probably due to urban heat island effect with rapid urbanization. The averaged temporal linear trend of insolation at 22 weather stations nationwide is about +1.47 W m^{-2} yr^{-1} despite the decreasing phase of solar cycle during the 2000s. This is possibly caused by reduction in particulate matter emissions due to enhanced environment regulation in South Korea during the recent decade (KMOE, 2012).

Although O_3 and related meteorological variables such as temperature and insolation have recently increased in South Korea, the spatial patterns of their temporal trends do not show clear similarity. In addition, the spatial distribution of O_3 trends is rather inhomogeneous even on a metropolitan scale. For instance, Table 1 shows a wide range of O_3 trends among the SMA cities from -1.25% yr^{-1} of Gwacheon to +2.82% yr^{-1} of Seoul. The spatial inhomogeneity in O_3 trend and the trend differences among O_3, temperature, and insolation imply that the long-term O_3 trends in South Korea are not only affected by changes in meteorological conditions but also influenced by changes in local precursor emissions or transport of O_3 and its precursors. The local effects of precursor emissions on the long-term changes in O_3 are further examined in Sect 3.6.

3.2. Relationships between O_3 and meteorological variables

A multiple linear regression model is here adopted to explain relationships between $O_{3\ 8h}$ and each of key meteorological variables such as T_{max}, SI, TD, PS, WS, and RH. To exclude day-to-day short-term fluctuations or white noises from the original time series, $KZ_{29,3}$ was applied to each variable before the regression process and yielded baselines of each variable. As a result of the multiple linear regression, coefficients of determination (R^2) between baselines of $O_{3\ 8h}$ and each meteorological variable, as well as

361 adjusted R^2 for the multiple linear regression models, were calculated for 72 air quality
362 monitoring sites distributed in 25 cities nationwide and summarized in Table 2. The
363 nationwide average of adjusted R^2 is 0.51 and that of R^2 is 0.50 for SI, 0.29 for PS, 0.22 for
364 T_{max}, 0.14 for TD, 0.05 for RH, and 0.03 for WS, respectively. In South Korea, SI, T_{max},
365 and TD generally show positive correlations with O_3 levels while PS is negatively
366 correlated with O_3 variations. Since the short-term variability in each variable is excluded,
367 the negative correlation between O_3 and PS is related to their seasonal cycle rather than
368 continuously changing weather system of high and low. PS in South Korea located on the
369 continental east coast is mostly affected by the cold continental high pressure air mass
370 during the winter when the O_3 concentrations are lowest. On the other hand, WS and RH
371 show weak correlations with O_3 variations.

372 The spatial distributions of R^2 for T_{max} and SI, as well as the adjusted R^2 for the
373 combined meteorological effects, are represented in Fig. 5. Both Figs. 5a and 5b show a
374 common spatial pattern with high correlations at the inland and SMA cities and low
375 correlations at the coastal cities. For instance, the average R^2 value with T_{max} for the
376 coastal cities is only 0.07, which is much smaller than 0.36 for the SMA cities and 0.30 for
377 the inland cities. Also, the average R^2 values with SI are 0.60 for the SMA cities and 0.58
378 for the inland cities, but 0.35 for the coastal cities. Despite the similar pattern between Figs.
379 5a and 5b, the R^2 values of SI are much higher than those of T_{max} because temperature
380 affects net O_3 production rather indirectly compared to the direct influence of insolation on
381 O_3 levels by photochemical production (Dawson et al., 2007; and references therein). The
382 apparent R^2 differences among three regions indicate that temporal variations of O_3 at the
383 SMA and inland cities are much more sensitive to SI and T_{max} than those at the coastal
384 cities. The low dependence of O_3 on T_{max} and SI at the coastal cities means that the
385 photochemical reactions of precursors are less important for determining O_3 levels there
386 compared to the SMA and inland cities.

387 The meteorological effects on O_3 at the inland, coastal, and SMA cities are also
388 examined by daily minimum O_3 ($O_{3\,min}$). As represented in Fig. 6a and Table 3, the $O_{3\,min}$
389 is high near the coast, low at the inland cities, and lowest in the SMA. In the polluted
390 urban area, the O_3 concentration reaches near-zero minima during the night since O_3 is
391 reduced by NO_x titration, nocturnal NO_y chemical process related to nitrate formation, and
392 dry deposition in the absence of photochemical production. However, in the coastal region
393 where the NO_x concentrations are low (Fig. 3b), the less titration and nitrate formation at
394 nighttime lead to the higher $O_{3\,min}$ levels. In addition, transport of O_3 from the regional

395 background could also keep high levels of O_3 during the night (Ghim and Chang, 2000).
396 Frequency distributions of O_3 concentrations in previous studies suggested that O_3 levels at
397 the coastal cities such as Gangneung, Jeju, Mokpo, Seosan, and Yeosu are affected by the
398 background O_3 transport, unlike Seoul where the effect of local precursor emission is
399 dominant (Ghim and Chang, 2000; Ghim, 2000). Therefore, combined effects of the low
400 NO_x levels and transport of the regional background O_3 influence the high $O_{3\,min}$ near the
401 coast.

402 Compared to the spatial distribution of R^2 between baselines of $O_{3\,8h}$ and T_{max} or
403 SI (Figs. 5a and 5b), $O_{3\,min}$ distribution in Fig. 6a shows high $O_{3\,min}$ at the coastal cities
404 where the R^2 is low and low $O_{3\,min}$ at the inland cities where the R^2 is high. These opposite
405 patterns suggest that the meteorological effects on the O_3 production are negatively
406 correlated with $O_{3\,min}$ for the South Korean cities. The clear negative correlations are also
407 shown in scatter plots (Figs. 6b and 6c). In both two scatter plots, the three geographical
408 groups of cities (blue for the coastal cities, green for the inland cities and red for SMA) are
409 well separated. Several industrial or metropolitan cities in the coastal region such as
410 Changwon (CW), Busan (BS), and Ulsan (US) have relatively low $O_{3\,min}$ compared to the
411 rest of coastal cities. Larger NO_x emissions in these southeastern coastal cities (Fig. 3b)
412 induce lower $O_{3\,min}$ levels via NO_x titration and nocturnal NO_y chemical process. Among
413 the SMA cities, on the other hand, Ganghwa (GH) has much higher $O_{3\,min}$ compared to
414 other SMA cities. Ganghwa is a rural county located on the northwestern coast of the SMA.
415 Therefore, both small NO_x emissions there and transport of regional background O_3 from
416 the Yellow Sea affect the characteristics of O_3 in Ganghwa.

417 The different meteorological effects on O_3 between the coastal and inland regions
418 are further examined with wind speed. Daily average wind speed (WS) data over South
419 Korea are averaged for 12 yr. The 12-yr averaged WS are summarized in Table 3 and
420 presented in spatial map of Fig. 7a, which show high wind speed in the coastal region and
421 low wind speed in the inland region. Figures 7b and c show that the averaged wind speeds
422 at 25 cities are positively correlated with $O_{3\,min}$ and negatively correlated with the R^2
423 between O_3 and T_{max}. In general, surface mixing and ventilation by high wind speeds
424 reduce the precursors near surface and thus decrease the photochemical production of O_3.
425 Therefore the relationship between high wind speed and high O_3 levels in the coastal
426 region is attributable to the transport of background O_3. On the other hand, the weaker
427 wind speed induces more effective photochemical reaction through the longer reaction
428 time in stagnant condition as well as more enhanced aerodynamic resistance to dry

deposition (Jacob and Winner, 2009). Therefore, the effects of insolation and temperature on the O_3 productions become more important in the inland region where the wind speeds are lower.

3.3. Probability of O_3 exceedances related to temperature

Evaluating the probability of O_3 exceeding the air quality standard in a given range of temperature is useful to speculate about potential sensitivity of O_3 concentration to climate change (Lin et al., 2001; Jacob and Winner, 2009). Here we calculate the probabilities that $O_{3\ 8h}$ exceeds the Korean air quality standard of 60 ppbv (KMOE, 2012) as a function of the daily maximum temperature (T_{max}) for the coastal, inland, and SMA cities. Similar to the analyses in Lin et al. (2001) for the contiguous United States, Fig. 8 shows that the probabilities of O_3 exceedances increase with T_{max} at the inland and SMA cities. For example, the probability of O_3 exceedances in the SMA is almost doubled by about 4°C increase in T_{max} and reach 27% at 30°C. In the coastal region, on the other hand, the probability of O_3 exceedance increases up to 12–13% with T_{max} change from 10°C to 20°C and does not increase significantly for T_{max} above 20°C. This is consistent with the spatial feature of the meteorological effects on O_3 levels, which are high at the inland and SMA cities and low at the coastal cities as described in the previous section. Therefore, the probability of high O_3 occurrence will be more sensitive to the future climate change at the inland and SMA cities than at the coastal cities. In the previous modeling study by Boo et al. (2006), T_{max} over the Korean peninsula is expected to rise by about 4–5°C to the end of 21st century owing to global warming. This indicates considerable future increases in exceedances of the O_3 air quality standard over South Korea except over coastal regions.

3.4. Relative contributions of O_3 variations in different time scales

Surface O_3 variation can be decomposed into short-term component ($[O_{3\ ST}]$), seasonal component ($[O_{3\ SEASON}]$), and long-term component ($[O_{3\ LT}]$) by using the KZ-filter as described in Sect. 2.2. We evaluated relative contributions of each component to total variance of original time series. Overall, the relative contributions of $[O_{3\ LT}]$ in Fig. 9c are much smaller than those of $[O_{3\ ST}]$ in Fig. 9a and $[O_{3\ SEASON}]$ in Fig. 9b at all cities (Table 4). Therefore, sum of $[O_{3\ ST}]$ and $[O_{3\ SEASON}]$ account for the most of O_3 variations.

In Figs. 9a and 9b, the relative contributions of $[O_{3\ ST}]$ and $[O_{3\ SEASON}]$ show a strong negative relationship spatially. The relative contributions of $[O_{3\ ST}]$ are generally larger at the coastal cities (53.1%) than at the inland cities (45.9%), whereas the relative

463 contributions of [$O_{3\ SEASON}$] are smaller at the coastal cities (32.8%) than at the inland
464 cities (41.9%).
465 Since [$O_{3\ ST}$] is related to synoptic-scale weather fluctuation (Rao et al., 1995; Rao
466 et al., 1997), the large relative contributions of [$O_{3\ ST}$] at the coastal cities indicate the
467 stronger effects of the eastward moving synoptic weather systems in there. Interestingly,
468 the highest value of [$O_{3\ ST}$] contribution is appeared at a northeastern coastal city,
469 Gangneung. High and steep mountains on the west of Gangneung induce often warm, dry,
470 and strong westerly winds, which is favorable to the clear sky and strong vertical mixing
471 over the region. Since the westerly winds contain the precursors emitted from the SMA,
472 the clear sky condition increases the O_3 levels during the daytime. In addition, the strong
473 vertical mixing of high O_3 air from the upper troposphere compensates the O_3 loss by
474 titration during the nighttime. In the easterly winds, however, orographic lift often forms
475 fogs or clouds over the region and reduces the photochemical production of O_3. Therefore,
476 combined effects of wind directions related to synoptic weather systems and topography
477 increase the short-term variability of O_3 at Gangneung.
478 On the other hand, [$O_{3\ SEASON}$] is driven mainly by the annual cycle of
479 meteorological factors such as insolation or temperature. Therefore, the large relative
480 contributions of [$O_{3\ SEASON}$] at the inland cities are consistent with the higher impacts of
481 temperature and insolation on the O_3 therein (Figs. 5 and 9b). The highest and second
482 highest values of [$O_{3\ SEASON}$] contribution are appeared at Andong and Wonju located in
483 the inland basin. Since the basin topography often traps pollutants and induces large
484 annual ranges of temperature, seasonal variability of O_3 at two cities is larger than that of
485 other inland cities.
486 [$O_{3\ LT}$] explain less than 10% of the total variances, but its relative contribution is
487 considerable in the southwestern part of the Korean peninsula as displayed in Fig. 9c. This
488 is related to relatively large long-term variability or trend in the region and is further
489 discussed in Sect. 3.6.
490
491 **3.5. Short-term variation of O_3 related to wind direction**
492 The short-term components of O_3 ([$O_{3\ ST}$]) account for a large fraction of total O_3
493 variation over South Korea. In Table 4, relative contributions of [$O_{3\ ST}$] range from 32.7%
494 to 62.5% and have a nationwide average of 49.8%. Therefore, it is no wonder that high O_3
495 episodes are mostly determined by day-to-day fluctuation of [$O_{3\ ST}$]. One considerable
496 factor influencing the short-term variation of O_3 is wind. Shin et al. (2012) displayed [O_3

497 $_{ST}$] on the wind speed-direction domain and showed that the effects of episodic long-range
498 transport and local precursor emission on the ambient O_3 concentrations could be
499 qualitatively separated from [$O_{3\ ST}$].

500 We here further investigate the transport effect on the short-term variations of O_3
501 and the frequency of high O_3 episodes using exp[$O_{3\ ST}$] and wind directions (WDs). As
502 described in Sect. 2.2, exp[$O_{3\ ST}$] is a ratio of the raw $O_{3\ 8h}$ concentration to its baseline
503 concentration in ppbv (exp[$O_{3\ BL}$]). Thus, the $O_{3\ 8h}$ concentration is higher than the
504 baseline $O_{3\ 8h}$ concentration when exp[$O_{3\ ST}$] > 1. We classified every single value of
505 exp[$O_{3\ ST}$] by 8 cardinal WDs during the months of frequent high O_3 events (May–
506 October) at all available monitoring sites within each city. The probabilities of exp[$O_{3\ ST}$]
507 > 1 by each WD were compared with the probabilities exceeding the South Korean air
508 quality standard of 60 ppbv for $O_{3\ 8h}$.

509 Figure 10 shows exp[$O_{3\ ST}$] in the SMA cities (Seoul, Incheon, Suwon, and
510 Ganghwa) with probabilities of exp[$O_{3\ ST}$] > 1 and $O_{3\ 8h}$ > 60 ppbv for each WD. In Seoul,
511 high O_3 episodes are occurred most in northwesterly although westerly and northeasterly
512 winds predominate during the months of frequent high O_3 events (Figs. 10a and 10b). The
513 high probability of high O_3 in northwesterly in Seoul is similar to those in other
514 neighboring cities in SMA, where the predominant probability also appears in
515 northwesterly wind in Incheon located in the west of Seoul (Figs. 10c and 10d), westerly
516 wind in Suwon in the south of Seoul (Figs. 10e and 10f), and Ganghwa in the northwest of
517 Seoul (Figs. 10g and 10h).

518 Sea-mountain breeze can explain the prevalence of high O_3 episodes under
519 westerly or northwesterly winds in the SMA. In the western coast of the SMA, there are
520 many thermoelectric power plants (see triangles in Figs. 11 and 12) and industrial
521 complexes, which directly emit a large amount of O_3 precursors. Heavy inland and
522 maritime transportation in those regions is also an important source of NO_x and
523 hydrocarbon emissions. Since the SMA is surrounded by the Yellow Sea in the west and
524 mountainous region in the east (see Fig. 1), the westerly sea breeze is well developed
525 under O_3-conducive meteorological conditions such as high temperature and strong
526 insolation with low wind speed (Ghim and Chang, 2000; Ghim et al., 2001). In addition,
527 locally emitted precursors and transported background O_3 from the west are trapped in the
528 SMA due to the westerly sea breeze and the mountainous terrain in the east of the SMA.
529 Therefore, the O_3 concentrations in the SMA increase in such O_3-conducive
530 meteorological conditions with near-westerly winds.

Another factor to increase the high O_3 probabilities in the near-westerly winds is long-range transport of O_3 and its precursors from China. For example, Ghim et al. (2001) reported some high O_3 cases in the SMA, which result from the transport of O_3-rich air with strong westerly wind at dawn under overcast conditions. Oh et al. (2010) also showed that the elevated layer of high O_3 concentration over the SMA is associated with the long-range transport of O_3 from eastern China. As the mixing layer thickens over the SMA, the O_3 concentration can increase by up to 25% via vertical down-mixing process (Oh et al., 2010). Recently, Kim et al. (2012) showed that westerly winds also transport O_3 precursors such as NO_2 and carbon monoxide (CO) from China to South Korea.

Interestingly, the high O_3 probability in Ganghwa (Figs. 10g and 10h) shows bimodal distribution with another peak in easterly wind. Considering that Ganghwa is a rural county on the northwestern coast of the SMA, the double peak of high O_3 probability in easterly and westerly winds shows the effects of both local and long-range transport.

We extended the above $\exp[O_{3\ ST}]$ and WDs analysis to 25 cities over South Korea. The nationwide view of the high O_3 probabilities is represented by the probabilities of $\exp[O_{3\ ST}] > 1$ and $O_{3\ 8h} > 60$ ppbv by each wind direction during the months of frequent high O_3 events (May–October). Figures 11 and 12 show spatial maps of the probabilities of $\exp[O_{3\ ST}] > 1$ and $O_{3\ 8h} > 60$ ppbv, respectively. As indicators of major precursor emission point source, we marked 26 of major thermoelectric power plants with triangles on the map. In general, the most of the thermoelectric power plants are located in the western coast of the SMA and southeastern coastal region of the Korean peninsula. Thermoelectric power plants are important sources of NO_x in South Korea, accounting for 13% (0.14 Mt) of total NO_x emission nationwide (KMOE, 2013). Considering that industrial complexes over South Korea are mostly concentrated near the power plants, the area with triangles in Figs. 11 and 12 represents major sources of O_3 precursors.

In Figs. 11 and 12, the both probabilities of $\exp[O_{3\ ST}] > 1$ and $O_{3\ 8h} > 60$ ppbv are generally high on a national scale in the near-westerly wind conditions (Figs. 11f–h and 12 f–h). The prevailing westerly wind of the synoptic-scale flow transports O_3 and its precursors from China to South Korea and thus increases the probability of high O_3 episodes as well as high O_3 concentrations. However, on a local scale, the high probability regions of high O_3 correspond to downwind of the thermoelectric power plants. For example, the high probabilities of high O_3 in the southeastern part of South Korea, downwind of power plants along the southeastern coast, also appear even in the easterly or southerly wind (Figs. 11c–e and 12c–e). Therefore, the spatial features of the high O_3

565 probabilities in each wind direction could be associated with both local effect of precursor
566 emission and long-range transport from the continent.
567
568 **3.6. Long-term variation of O_3 and local precursor emissions**
569 The temporal linear trend of baseline ($[O_{3\,BL}]$) is almost the same as that of the
570 original time series since short-term component ($[O_{3\,ST}]$) is nearly detrended. Therefore,
571 the O_3 trend can be represented as a sum of the seasonal component ($[O_{3\,SEASON}]$) and
572 long-term component ($[O_{3\,LT}]$) trends. The spatial trend distributions of $[O_{3\,BL}]$ and its two
573 separated components of seasonal and long-term components are shown in Fig. 13. It is
574 noted that the period used in Fig. 13 is shorter than the total period of original data because
575 of truncation effect in the KZ-filter process. The long-term component obtained by the
576 KZ-filter of $KZ_{365,3}$ loses 546 days at the beginning and end of original time series.
577 The increasing trends of O_3 are generally high in the SMA and southwestern part
578 and low in the southeastern coastal region of Korean peninsula (Fig. 13a). This spatial
579 inhomogeneity of the O_3 trends over South Korea is mainly contributed by the long-term
580 component trends (Fig. 13c) rather than the seasonal component trend (Fig. 13b).
581 Therefore, the large spatial variability in local precursor emissions induced the spatial
582 inhomogeneity of O_3 trends in South Korea. On the other hand, relatively homogeneous
583 distribution of the seasonal component trends implies that meteorological influences on the
584 long-term changes in O_3 have little regional dependence nationwide.
585 Since the spatially inhomogeneous O_3 trends are related to the local precursor
586 emissions, we also tried to investigate their relationship with NO_2 measurement data. To
587 detect temporally synchronous and spatially coupled patterns between the long-term
588 variations of O_3 and NO_2, we applied the SVD to $[O_{3\,LT}]$ and the long-term component of
589 NO_2 ($[NO_{2\,LT}]$). $[NO_{2\,LT}]$ was simply obtained by applying the KZ-filter of $KZ_{365,3}$ to the
590 log-transformed NO_2 time series. The SVD is usually applied to two combined space-time
591 data fields, based on the computation of a temporal cross-covariance matrix between two
592 data fields. The SVD identifies coupled spatial patterns and their temporal variations, with
593 each pair of spatial patterns explaining a fraction of the squared covariance between the
594 two space-time data sets. The squared covariance fraction (SCF) is largest in the first pair
595 (mode) of the patterns, and each succeeding mode has a maximum SCF that is unexplained
596 by the previous modes.
597 The first three leading SVD modes (singular vectors) of the coupled O_3 and NO_2
598 long-term components account for the SCF with 94.6% of the total, of which the first,

second, and third modes are 63.7%, 23.6%, and 7.3% respectively. Figure 14 displays the expansion coefficients (coupled spatial patterns) and their time series of the first mode along with spatial map of the [$NO_{2\,LT}$] trends. The dominant first mode of the O_3 and NO_2 long-term components (Figs. 14a and 14b) is very similar to the spatial distributions of [$O_{3\,LT}$] trends (Fig. 13c) and [$NO_{2\,LT}$] trends (Fig. 14c) respectively. In Fig. 14d, the strong coherence in the time series is observed between the first modes of the [$O_{3\,LT}$] and [$NO_{2\,LT}$] with a correlation coefficient of 0.98. The results of SVD analysis suggest that the long-term variations of O_3 and NO_2 in South Korea have similar temporal evolutions with different spatial patterns.

The differences in spatial patterns of [$O_{3\,LT}$] and [$NO_{2\,LT}$] as shown in Figs 14a and 14b are required to be further investigated. Since the VOCs emissions from industry, transportation, and the solvent usage in construction are large in South Korea (KMOE, 2013), further analyses of VOCs measurements are needed. On top of that, especially in South Korea, biogenic precursor emissions are also potentially important for the analysis due to dense urban vegetation in and around metropolitan areas. Therefore, there remains the limitation of our current data analysis due to the lack of both VOC emission data and observations of atmospheric concentrations of VOCs in South Korea.

4. Conclusion

This study has investigated various spatio-temporal features and inter-relationship of surface O_3 and related meteorological variables over South Korea based on ground measurements for the period 1999–2010. A general overview of surface O_3 in terms of spatial distributions and its temporal trend is provided based on its decomposed components by the KZ-filter.

In South Korea, the O_3 concentrations are low at the inland and SMA cities due to the NO_x titration by anthropogenic emissions and high at the coastal cities possibly due to the dynamic effects of the sea breeze. The averaged O_3 levels in South Korea have increased for 1999–2010 with an averaged temporal linear trend of +0.26 ppbv yr^{-1} (+1.15% yr^{-1}). The recent increase of the O_3 levels in East Asia may result from the recent increase of anthropogenic precursor emissions and the long-term variations in meteorological effects.

We applied a linear regression model to investigate the relationships between O_3 and meteorological variables such as temperature, insolation, dew-point temperature, sea-level pressure, wind speed, and relative humidity. Spatial distribution of the R^2 values

633 shows high meteorological influences in the SMA and inland regions and low
634 meteorological influences in the coastal region. The high meteorological influences in the
635 SMA and inland regions are related to effective photochemical activity, which results from
636 large local precursor emissions and stagnant conditions with low wind speeds. On the
637 other hand, the low meteorological influences in the coastal region are related to large
638 transport effects of the background O_3 and ventilation and dry deposition with high wind
639 speeds.

640 In the SMA and inland region, the high O_3 probability ($O_{3\ 8h} > 60$ ppbv) increases
641 with the daily maximum temperature rise. Specifically in the SMA, the most populated
642 area in South Korea, the probability of the O_3 exceedances is almost doubled for about 4°C
643 increase in daily maximum temperature and reached 27% at 30°C. It is noted that the
644 variations in O_3 exceedance probabilities according to the maximum temperature show an
645 approximate logarithmic increase in the SMA and inland regions. It thus implies that these
646 regions will experience more frequent high O_3 events in the future climate conditions with
647 the increasing global temperature.

648 The O_3 time series observed at each monitoring site can be decomposed into the
649 short-term, seasonal, and long-term components by the KZ-filter. Relative contributions of
650 each separated component show that the short-term and seasonal variations account for
651 most of the O_3 variability. Relative contributions of the short-term component are large at
652 the coastal cities due to influence of the background O_3 transport. In contrast, those of the
653 seasonal component are large at the inland cities due to the high meteorological influences
654 on the O_3 variations.

655 The transport effects on the short-term component are shown in the probability
656 distributions of both high short-term component values and O_3 exceedances for each wind
657 direction. During the months of frequent high O_3 events (May–October) in South Korea,
658 the probabilities of both high short-term component O_3 and O_3 exceedances are higher in
659 the near-westerly wind condition rather than in other wind directions. For the short-term
660 time scale, the eastward long-range transport of O_3 and precursors from China can cause
661 the nationwide high probabilities of O_3 exceedances in the near-westerly wind condition.
662 However, the high probabilities of O_3 extreme events in downwind regions of the
663 thermoelectric power plants and industrial complexes are related to local transport of O_3
664 precursors which apparently enhances the O_3 levels.

665 The distribution of O_3 trends in South Korea is spatially inhomogeneous.
666 Although the relative contributions of the long-term components are much smaller than

667 those of other two components, such spatially inhomogeneous distribution of O_3 trend is
668 mainly contributed by the long-term component O_3 trends rather than the seasonal
669 component O_3 trend related to the long-term change of meteorological conditions. It is
670 because the long-term change of the local precursor emission has a localized effect on the
671 long-term O_3 change. SVD between O_3 and NO_2 shows that the long-term variations of O_3
672 and NO_2 in South Korea have similar temporal evolutions with different spatial patterns.
673 The results of SVD analysis clearly demonstrate the influences of local precursor
674 emissions on the long-term changes in O_3. However, the precise interpretation of the large
675 spatially inhomogeneous distribution in the long-term component O_3 trend is limited due
676 to lack of VOC measurements data.
677 The KZ-filter is a useful diagnostic tool to reveal the spatio-temporal features of
678 O_3 and its relationship with meteorological variables. General features revealed by the KZ-
679 filter analysis will provide a better understanding of spatial and temporal variations of
680 surface O_3 as well as possible influences of local emissions, transport, and climate change
681 on O_3 levels in South Korea. Our analyses would also be helpful as a reference for the
682 evaluation of chemistry transport models and furthermore for establishing appropriate O_3
683 control policy.
684
685 **Acknowledgements**
686 This study has been funded by the Green City Technology Flagship Program of the Korea
687 Institute of Science and Technology. Daeok Youn was supported by Chungbuk National
688 University. This work was done as Huikyo Lee's private venture and not in the author's
689 capacity as an employee of the Jet Propulsion Laboratory, California Institute of
690 Technology.
691

692 **References**

693 Akimoto, H.: Global air quality and pollution, Science, 302, 1716–1719,
694 doi:10.1126/science.1092666, 2003.

695 Bell, M. L., Goldberg, R., Hogrefe, C., Kinney, P. L., Knowlton, K., Lynn, B., Rosenthal,
696 J., Rosenzweig, C., and Patz., J. A.: Climate change, ambient ozone, and health in 50
697 US cities, Climatic Change, 82, 61–76, doi:10.1007/s10584-006-9166-7, 2007.

698 Bernard, S. M., Samet, J. M., Grambsch, A., Ebi, K. L., and Romieu, I.: The potential
699 impacts of climate variability and change on air pollution-related health effects in the
700 United States, Environ. Health Persp., 109, 199–209, 2001.

701 Boo, K.-O., Kwon, W.-T., and Baek, H.-J.: Change of extreme events of temperature and
702 precipitation over Korea using regional projection of future climate change, Geophys.
703 Res. Lett., 33, L01701, doi:10.1029/2005GL023378, 2006.

704 Camalier, L., Cox, W., and Dolwick, P.: The effects of meteorology on ozone in urban
705 areas and their use in assessing ozone trends, Atmos. Environ., 41, 7127–7137, doi:
706 10.1016/j.atmosenv.2007.04.061, 2007.

707 Carmichael, G. R., Uno, I., Phadnis, M. J., Zhang, Y., and Sunwoo, Y.: Tropospheric
708 ozone production and transport in the springtime in East Asia, J. Geophys. Res., 103,
709 10649–10671, doi:10.1029/97JD03740, 1998.

710 Chatani, S. and Sudo, K.: Influences of the variation in inflow to East Asia on surface
711 ozone over Japan during 1996-2005, Atmos. Chem. Phys., 11, 8745–8758,
712 doi:10.5194/acp-11-8745-2011, 2011.

713 Dawson, J. P., Adams, P. J., and Pandis, S. N.: Sensitivity of ozone to summertime climate
714 in the eastern USA: A modeling case study, Atmos. Environ., 41, 1494–1511,
715 doi:10.1016/j.atmosenv.2006.10.033, 2007.

716 Dibb, J. E., Talbot, R. W., Scheuer, E., Seid, G., DeBell, L., Lefer, B., and Ridley, B.:
717 Stratospheric influence on the northern North American free troposphere during
718 TOPSE: ^{7}Be as a stratospheric tracer, J. Geophys. Res., 108, 8363,
719 doi:10.1029/2001JD001347, 2003.

720 Diem, J. E.: A critical examination of ozone mapping from a spatial-scale perspective,
721 Environ. Pollut., 125, 369–383, doi:10.1016/S0269-7491(03)00110-6, 2003.

722 Ding, A. J., Wang, T., Thouret, V., Cammas, J.-P., and Nédélec, P.: Tropospheric ozone
723 climatology over Beijing: analysis of aircraft data from the MOZAIC program,
724 Atmos. Chem. Phys., 8, 1–13, doi:10.5194/acp-8-1-2008, 2008.

725 Eskridge, R. E., Ku, J. Y., Rao, S. T., Porter, P. S., and Zurbenko, I. G.: Separating
726 different scales of motion in time scales of motion in time series of meteorological
727 variables, B. Am. Meteorol. Soc., 78, 1473–1483, doi:10.1175/1520-
728 0477(1997)078<1473:SDSOMI>2.0.CO;2, 1997.
729 Flaum, J. B., Rao, S. T., and Zurbenko, I. G.: Moderating the influence of meteorological
730 conditions on ambient ozone concentrations, J. Air Waste Manage., 46, 35–46,
731 doi:10.1080/10473289.1996.10467439, 1996.
732 Gardner, M. W. and Dorling, S. R.: Meteorologically adjusted trends in UK daily
733 maximum surface ozone concentrations, Atmos. Environ., 34, 171–176,
734 doi:10.1016/S1352-2310(99)00315-5, 2000.
735 Ghim, Y. S.: Trends and factors of ozone concentration variations in Korea, Journal of
736 Korean Society for Atmospheric Environment, 16, 607–623, 2000. (In Korean)
737 Ghim, Y. S. and Chang, Y. S.: Characteristics of ground-level ozone distribution in Korea
738 for the period of 1990-1995, J. Geophys. Res., 105, 8877–8890,
739 doi:10.1029/1999JD901179, 2000.
740 Ghim, Y. S., Oh, H. S., and Chang, Y. S.: Meteorological effects on the evolution of high
741 ozone episodes in the Greater Seoul Area, J. Air Waste Manage., 51, 185–202,
742 doi:10.1080/10473289.2001.10464269, 2001.
743 Guicherit, R. and Roemer, M.: Tropospheric ozone trends, Chemosphere-Global Change
744 Science, 2, 167–183, 2000.
745 Ibarra-Berastegi, G., Madariaga, I., Elías, A., Agirre, E., and Uria, J.: Long-term changes
746 of ozone and traffic in Bilbao, Atmos. Environ., 35, 5581–5592, doi:10.1016/S1352-
747 2310(01)00210-2, 2001.
748 IPCC (Intergovernmental Panel on Climate Change): Climate Change 2007: The Physical
749 Scientific Basis: Contribution of Working Group I to the Fourth Assessment Report
750 of the Intergovernmental Panel on Climate Change, edited by: Solomon, S., Qin, D.,
751 Manning, M., Chen, Z., Marquis, M., Averyt, K. B., Tignor, M., and Miller, H. L.,
752 Cambridge University Press, Cambridge, United Kingdom and New York, NY, USA,
753 2007.
754 Jacob, D. J., Logan, J. A., and Murti, P. P.: Effect of rising Asian emissions on surface
755 ozone in the United States, Geophys. Res. Lett., 26, 2175–2178,
756 doi:10.1029/1999GL900450, 1999.
757 Jacob, D. J. and Winner, D. A.: Effect of climate change on air quality, Atmos. Environ.,
758 43, 51–63, doi:10.1016/j.atmosenv.2008.09.051, 2009.

759 Jaffe, D. A., Parrish, D., Goldstein, A., Price, H., and Harris, J.: Increasing background
760 ozone during spring on the west coast of North America, J. Geophys. Res., 30, 1613,
761 doi:10.1029/2003GL017024, 2003.
762 Jin, L., Lee, S.-H., Shin, H.-J., and Kim, Y. P.: A study on the ozone control strategy using
763 the OZIPR in the Seoul Metropolitan Area, Asian J. Atmos. Environ., 6, 111–117,
764 doi:10.5572/ajae.2012.6.2.111, 2012.
765 Kim, J. Y., Kim, S.-W., Ghim, Y. S., Song, C. H., and Yoon, S.-C.: Aerosol properties at
766 Gosan in Korea during two pollution episodes caused by contrasting weather
767 conditions, Asia-Pacific J. Atmos. Sci., 48(1), 25–33, doi:10.1007/s13143-012-0003-
768 9, 2012.
769 KMOE (Ministry of Environment, Korea): Annual report of ambient air quality in Korea,
770 2011, 11-1480523-000198-10, National Institute of Environmental Research,
771 Environmental Research Complex, Incheon, 2012. (In Korean, available at:
772 http://webbook.me.go.kr/DLi-File/091/012/5515496.PDF)
773 KMOE (Ministry of Environment, Korea): Air pollutants emission (1999–2010), 11-
774 1480523-001377-01, National Institute of Environmental Research, Environmental
775 Research Complex, Incheon, 2013. (In Korean, available at:
776 http://webbook.me.go.kr/DLi-File/NIER/09/018/5553596.pdf)
777 Lei, H., Wuebbles, D. J., Liang, X.-Z., and Olsen, S.: Domestic versus international
778 contributions on 2050 ozone air quality: How much is convertible by regional
779 control?, Atmos. Environ., 68, doi:10.1016/j.atmosenv.2012.12.002, 2013.
780 Lei, H. and Wang, J. X. L.: Sensitivities of NO_x transformation and the effects on surface
781 ozone and nitrate, Atmos. Chem. Phys., 14, 1385–1396, doi:10.5194/acp-14-1385-
782 2014, 2014.
783 Levy, H., Mahlman, J., Moxim, W. J., and Liu, S.: Tropospheric ozone: the role of
784 transport, J. Geophys. Res., 90, 3753–3772, doi:10.1029/JD090iD02p03753, 1985.
785 Levy, J. I., Chemerynski, S. M., and Sarnat, J. A.: Ozone exposure and mortality: an
786 empiric Bayes metaregression analysis, Epidemiology, 16, 458–468, doi:
787 10.1097/01.ede.0000165820.08301.b3, 2005.
788 Lin, C. Y. C., Jacob, D. J., and Fiore, A. M.: Trends in exceedances of the ozone air
789 quality standard in the continental United States, 1980-1998, Atmos. Environ., 35,
790 3217–3228, doi:10.1016/S1352-2310(01)00152-2, 2001.
791 Lin, J.-T., Patten, K. O., Hayhoe, K., Liang, X.-Z., and Wuebbles, D. J.: Effects of future
792 climate and biogenic emissions changes on surface ozone over the United States and

China, J. Appl. Meteorol. Clim., 47, 1888–1909, doi:10.1175/2007JAMC1681.1, 2008.

Liu, S. C., Trainer, M., Fehsenfeld, F. C., Parrish, D. D., Williams, E. J., Fahey, D. W., Hübler, G., and Murphy, P. C.: Ozone production in the rural troposphere and the implications for regional and global ozone distributions, J. Geophys. Res., 92, D4, 4191–4207, doi:10.1029/JD092iD04p04191, 1987.

Logan, J. A.: Tropospheric ozone: seasonal behavior, trends and anthropogenic influence, J. Geophys. Res., 90, 463–482, doi:10.1029/JD090iD06p10463, 1985.

Lu, H. C. and Chang, T. S.: Meteorologically adjusted trends of daily maximum ozone concentrations in Taipei, Taiwan, Atmos. Environ., 39, 6491–6501, doi:10.1016/j.atmosenv.2005.06.007, 2005.

Lu, G. Y. and Wong, D. W.: An adaptive inverse-distance weighting spatial interpolation technique, Comput. Geosci., 34, 1044–1055, doi:10.1016/j.cageo.2007.07.010, 2008.

Mickley, L. J., Jacob, D. J., and Field, B. D.: Climate response to the increase in tropospheric ozone since preindustrial times: A comparison between ozone and equivalent CO_2 forcings, J. Geophys. Res., 109, D05106, doi:10.1029/2003JD003653, 2004.

Milanchus, M. L., Rao, S. T., and Zurbenko, I. G.: Evaluating the effectiveness of ozone management efforts in the presence of meteorological variability, J. Air Waste Manage., 48, 201–215, doi:10.1080/10473289.1998.10463673, 1998.

Nagashima, T., Ohara, T., Sudo, K., and Akimoto, H.: The relative importance of various source regions on East Asian surface ozone, Atmos. Chem. Phys., 10, 11305–11322, doi:10.5194/acp-10-11305-2010, 2010.

Oh, I. B., Kim, Y. K., Lee, H. W., and Kim, C. H.: An observational and numerical study of the effects of the late sea breeze on ozone distributions in the Busan metropolitan area, Korea, Atmos. Environ., 40, 1284–1298, doi:10.1016/j.atmosenv.2005.10.049, 2006.

Oh, I. B., Kim, Y. K., Hwang, M. K., Kim, C. H., Kim, S., and Song, S. K.: Elevated ozone layers over the Seoul Metropolitan Region in Korea: Evidence for long-range ozone transport from eastern China and its contribution to surface concentrations, J. Appl. Meteorol. Clim., 49, 203–220, doi:10.1175/2009JAMC2213.1, 2010.

Olszyna, K. J., Luria, M., and Meagher, J. F.: The correlation of temperature and rural ozone levels in southeastern U.S.A., Atmos. Environ., 31, 3011–3022, doi:10.1016/S1352-2310(97)00097-6, 1997.

827 Oltmans, S. J., Lefohn, A. S., Scheel, H. E., Harris, J. M., Levy II, H., Galbally, I. E.,
828 Brunke, E.-G., Meyer, C. P., Lathrop, J. A., Johnson, B. J., Shadwick, D. S., Cuevas,
829 E., Schmidlin, F. J., Tarasick, D. W., Claude, H., Kerr, J. B., Uchino, O., and Mohnen,
830 V.: Trends of ozone in the troposphere, Geophys. Res. Lett., 25, 139–142,
831 doi:10.1029/97GL03505, 1998.
832 Oltmans, S. J., Lefohn, A. S., Harris, J. M., Galbally, I., Scheel, H. E., Bodeker, G.,
833 Brunke, E., Claude, H., Tarasick, D., Johnson, B. J., Simmonds, P., Shadwick, D.,
834 Anlauf, K., Hayden, K., Schmidlin, F., Fujimoto, T., Akagi, K., Meyer, C., Nichol, S.,
835 Davies, J., Redondas, A., and Cuevas, E.: Long-term changes in tropospheric ozone,
836 Atmos. Environ., 40, 3156–3173, doi:10.1016/j.atmosenv.2006.01.029, 2006.
837 Oltmans, S. J., Lefohn, A. S., Shadwick, D., Harris, J. M., Scheel, H. E., Galbally, I.,
838 Tarasick, D. W., Johnson, B. J., Brunke, E.-G., Claude, H., Zeng, G., Nichol, S.,
839 Schmidlin, F., Davies, J., Cuevas, E., Redondas, A., Naoe, H., Nakano, T., and
840 Kawasato, T.: Recent tropospheric ozone changes – A pattern dominated by slow or
841 no growth, Atmos. Environ., 67, 331–351, doi:10.1016/j.atmosenv.2012.10.057, 2013.
842 Ordóñez, C., Mathis, H., Furger, M., Henne, S., Hüglin, C., Staehelin, J., and Prévôt, A. S.
843 H.: Changes of daily surface ozone maxima in Switzerland in all seasons from 1992
844 to 2002 and discussion of summer 2003, Atmos. Chem. Phys., 5, 1187–1203,
845 doi:10.5194/acp-5-1187-2005, 2005.
846 Racherla, P. N. and Adams, P. J.: Sensitivity of global tropospheric ozone and fine
847 particulate matter concentrations to climate change, J. Geophys. Res., 111, D24103,
848 doi:10.1029/2005JD006939, 2006.
849 Rao, S. T. and Zurbenko, I. G.: Detecting and tracking changes in ozone air quality, J. Air
850 Waste Manage., 44, 1089–1092, doi:10.1080/10473289.1994.10467303, 1994.
851 Rao, S. T., Zalewsky, E., and Zurbenko, I. G.: Determining temporal and spatial variations
852 in ozone air quality, J. Air Waste Manage., 45, 57–61,
853 doi:10.1080/10473289.1995.10467342, 1995.
854 Rao, S. T., Zurbenko, I. G., Neagu, R., Porter, P. S., Ku, J. Y., and Henry, R. F.: Space and
855 time scales in ambient ozone data, B. Am. Meteorol. Soc., 78, 2153–2166,
856 doi:10.1175/1520-0477(1997)078<2153:SATSIA>2.0.CO;2, 1997.
857 Rasmussen, D. J., Fiore, A. M., Naik, V., Horowitz, L. W., McGinnis, S. J., and Schultz,
858 M. G.: Surface ozone-temperature relationships in the eastern US: A monthly
859 climatology for evaluating chemistry-climate models, Atmos. Environ., 47, 142–153,
860 doi:10.1016/j.atmosenv.2011.11.021, 2012.

Shin, H. J., Cho, K. M., Han, J. S., Kim, J. S., and Kim, Y. P.: The effects of precursor emission and background concentration changes on the surface ozone concentration over Korea, Aerosol Air Qual. Res., 12, 93–103, doi:10.4209/aaqr.2011.09.0141, 2012.

Sillman, S. and Samson, P. J.: Impact of temperature on oxidant photochemistry in urban, polluted rural and remote environments, J. Geophys. Res., 100, 11497–11508, doi:10.1029/94JD02146, 1995.

Tang, G., Wang, Y., Xin, J., and Ren, X.: Surface ozone trend details and interpretations in Beijing, 2001–2006, Atmos. Chem. Phys., 9, 8813–8823, doi:10.5194/acp-9-8813-2009, 2009.

Tanimoto, H., Sawa, Y., Matsueda, H., Uno, I., Ohara, T., Yamaji, K., Kurokawa, J., and Yonemura, S.: Significant latitudinal gradient in the surface ozone spring maximum over East Asia, Geophys. Res. Lett., 32, L21805, doi:10.1029/2005GL023514, 2005.

Tanimoto, H., Ohara, T., and Uno, I.: Asian anthropogenic emissions and decadal trends in springtime tropospheric ozone over Japan: 1998–2007, Geophys. Res. Lett., 36, L23802, doi:10.1029/2009GL041382, 2009.

Thompson, M. L., Reynolds, J. R., Cox, L. H., Guttorp, P., and Sampson, P. D.: A review of statistical methods for the meteorological adjustment of tropospheric ozone, Atmos. Environ., 35, 617–630, doi:10.1016/S1352-2310(00)00261-2, 2001.

Tilmes, S. and Zimmermann, J.: Investigation on the spatial scales of the variability in measured near-ground ozone mixing ratios, Geophys. Res. Lett., 25, 3827–3830, doi:10.1029/1998GL900034, 1998.

Tsakiri, K. G. and Zurbenko, I. G.: Prediction of ozone concentrations using atmospheric variables, Air Quality, Atmosphere & Health, 4, 111–120, doi:10.1007/s11869-010-0084-5, 2011.

Vingarzan, R.: A review of surface ozone background levels and trends, Atmos. Environ., 38, 3431-3442, doi:10.1016/j.atmosenv.2004.03.030, 2004.

Wang, T., Wei, X. L., Ding, A. J., Poon, C. N., Lam, K. S., Li, Y. S., Chan, L. Y., and Anson, M.: Increasing surface ozone concentrations in the background atmosphere of Southern China, 1994–2007, Atmos. Chem. Phys., 9, 6217–6227, doi:10.5194/acp-9-6217-2009, 2009.

Wang, X. and Mauzerall, D. L.: Characterizing distributions of surface ozone and its impact on grain production in China, Japan and South Korea: 1990 and 2020, Atmos. Environ., 38, 4383–4402, doi:10.1016/j.atmosenv.2004.03.067, 2004.

Wang, Y., Konopka, P., Liu, Y., Chen, H., Müller, R., Plöger, F, Riese, M., Cai, Z., and Lü, D.: Tropospheric ozone trend over Beijing from 2002–2010: ozonesonde measurements and modeling analysis, Atmos. Chem. Phys., 12, 8389–8399, doi:10.5194/acp-12-8389-2012, 2012.

Wise, E. K. and Comrie, A. C.: Extending the Kolmogorov-Zurbenko filter: Application to ozone, particulate matter, and meteorological trends, J. Air Waste Manage., 55, 1208–1216, doi:10.1080/10473289.2005.10464718, 2005.

Zhao, B., Wang, S. X., Liu, H., Xu, J. Y., Fu, K., Klimont, Z., Hao, J. M., He, K. B., Cofala, J., and Amann, M.: NO_x emissions in China: historical trends and future perspectives, Atmos. Chem. Phys., 13, 9869–9897, doi:10.5194/acp-13-9869-2013, 2013.

Table and Figure captions

Table 1. 12-yr averaged concentrations and temporal linear trends of daily average O_3 ($O_{3\ avg}$) at 46 cities over South Korea for the period 1999–2010. The cities are categorized into three groups: 16 coastal cities, 14 inland cities, and 16 cities in the Seoul Metropolitan Area (SMA).

Table 2. Coefficients of determination (R^2) between baseline of daily maximum 8-h average O_3 ($O_{3\ 8h}$) and baselines of six meteorological variables (T_{max}, SI, TD, PS, WS, and RH) at 25 cities over South Korea for the period 1999–2010. Adjusted R^2 (*Adj.* R^2) between baseline of $O_{3\ 8h}$ and combined meteorological effects ($a_0 + \sum_i a_i\ \mathrm{MET}_{BL}(t)_i$) are also represented. The cities are categorized into three groups: 10 coastal cities, 11 inland cities, and 4 cities in the Seoul Metropolitan Area (SMA). Numbers in bold fonts indicate correlations significant at the 95% level or higher.

Table 3. 12-yr averaged of daily minimum O_3 ($O_{3\ min}$) concentrations and daily average wind speeds (WS) at 46 cities over South Korea for the period 1999–2010. The cities are categorized into three groups: 16 coastal cities, 14 inland cities, and 16 cities in the Seoul Metropolitan Area (SMA).

Table 4. Relative contributions (%) of short-term components ($[O_{3\ ST}]$), seasonal components ($[O_{3\ SEASON}]$), and long-term components ($[O_{3\ LT}]$) to total variance of log-transformed daily maximum 8-h average O_3 ($[O_3]$) at 25 cities over South Korea for the period 1999–2010. The cities are categorized into three groups: 10 coastal cities, 11 inland cities, and 4 cities in the Seoul Metropolitan Area (SMA).

Figure 1. (a) Geographical locations of South Korea, and (b) 72 weather stations of the Korea Meteorological Administration (KMA) with blue circles, (c) 124 air quality monitoring sites of the National Institute of Environmental Research (NIER) with black dots, and (d) 72 air quality monitoring sites of NIER, which are located within 10 km from 25 weather stations of KMA over the South Korean domain.

Figure 2. Time series of daily maximum 8-h average ozone ($O_{3\ 8h}$) at the City Hall of Seoul and its separated components such as (a) log-transformed $O_{3\ 8h}$ time series ($[O_3]$) and its baseline ($[O_{3\ BL}]$), (b) short-term component ($[O_{3\ ST}]$), (c) seasonal component ($[O_{3\ SEASON}]$), and (d) long-term component ($[O_{3\ LT}]$) by applying KZ-filter. It is noted that the longer window length causes the larger truncation of the result (Wise and Comrie, 2005) since the KZ-filter is an iterative moving average process. The baseline in red solid line is superimposed in (a).

Figure 3. Spatial distributions of 12-yr averaged concentrations of (a) daily average O_3 ($O_{3\ avg}$) and (b) daily average nitrogen dioxide ($NO_{2\ avg}$), and (c) temporal linear trends of $O_{3\ avg}$ for the period 1999–2010 using data from 124 air quality monitoring sites (black dots) of NIER.

Figure 4. Spatial distributions of temporal linear trends of (a) daily average temperature (T) and (b) daily average surface insolation (SI) for the period 1999–2010 using data from 72 and 22 weather stations (black dots) of KMA, respectively.

Figure 5. Spatial distributions of squared correlation coefficients (R^2) between baselines of $O_{3\ 8h}$ ($[O_{3\ BL}]$) and (a) daily maximum temperature ($T_{max\ BL}$) and (b) surface insolation ($SI_{\ BL}$). Black dots represent 72 air quality monitoring sites of NIER. (c) Spatial distribution of adjusted R^2 between $[O_{3\ BL}]$ and combined meteorological effects ($a_0 + \sum_i a_i\ \mathrm{MET}_{BL}(t)_i$).

Figure 6. (a) Spatial distribution of 12-yr averaged concentrations of daily minimum O_3 ($O_{3\,min}$) for the period 1999–2010 using data from 124 air quality monitoring sites (black dots) of NIER. (b) Scatter plot of R^2 between [$O_{3\,BL}$] and $T_{max\,BL}$ versus $O_{3\,min}$ at 25 cities. (c) Scatter plot of R^2 between [$O_{3\,BL}$] and SI_{BL} versus $O_{3\,min}$ at 17 cities. City codes in red, green, and blue indicate the Seoul Metropolitan Area (SMA), inland, and coastal cities, respectively.

Figure 7. (a) Spatial distribution of 12-yr averaged daily average wind speeds (WS) for the period 1999–2010 using data from 72 weather stations (black dots) of KMA. (b) Scatter plot of $O_{3\,min}$ versus WS at 25 cities. (c) Scatter plot of R^2 between [$O_{3\,BL}$] and $T_{max\,BL}$ versus WS at 25 cities. City codes in red, green, and blue indicate the Seoul Metropolitan Area (SMA), inland, and coastal cities, respectively.

Figure 8. Probabilities of O_3 exceedances in the given range of daily maximum temperature (T_{max}) that $O_{3\,8h}$ will exceed air quality standard of South Korea (60 ppbv).

Figure 9. Spatial distributions of relative contributions of (a) short-term component ([$O_{3\,ST}$]), (b) seasonal component ([$O_{3\,SEASON}$]), and (c) long-term component ([$O_{3\,LT}$]) to the total variance of original time series ([O_3]) using data from 72 air quality monitoring sites (black dots) of NIER. Note that the color scales are all different.

Figure 10. Relationships between wind directions (WD) and exponentials of short-term components (exp[$O_{3\,ST}$]) during the months of frequent high O_3 events (May–October) at Seoul (a–b), Incheon (c–d), Suwon (e–f), and Ganghwa (g–h) in the Seoul Metropolitan Area (SMA) are represented in scatter plots of exp[$O_{3\,ST}$] versus WD (a, c, e, and g) and probabilities of O_3 exceedances in each WD (b, d, f, and h). Red dots in scatter plots denote high O_3 episodes that daily maximum 8-h average O_3 ($O_{3\,8h}$) will exceed air quality standard of South Korea (60 ppbv). Dashed lines in scatter plots denote the reference of exp[$O_{3\,ST}$] = 1. Probabilities of exp[$O_{3\,ST}$] > 1 and $O_{3\,8h}$ > 60 ppbv in each WD are represented as black thick lines and red thick lines, respectively. 95% of confidence intervals for each probability are represented as black and red thin lines. We used O_3 data from 12 sites in Seoul, 6 sites in Incheon, 3 sites in Suwon, and 1 site in Ganghwa.

Figure 11. Spatial distributions of probabilities that exponentials of the short-term components will exceed 1 (exp[$O_{3\,ST}$] > 1) for each wind direction (WD) of (a) northerly (N), (b) northeasterly (NE), (c) easterly (E), (d) southeasterly (SE), (e) southerly (S), (f) southwesterly (SW), (g) westerly (W), and (h) northwesterly (NW), respectively. Black dots denote 25 weather stations of KMA and triangles denote 26 major thermoelectric power plants in South Korea (blue triangle < 1000 MW, red triangles ≥ 1000 MW).

Figure 12. Spatial distributions of probabilities that daily maximum 8-h average O_3 ($O_{3\,8h}$) will exceed air quality standard of South Korea (60 ppbv) for each wind direction (WD) of (a) northerly (N), (b) northeasterly (NE), (c) easterly (E), (d) southeasterly (SE), (e) southerly (S), (f) southwesterly (SW), (g) westerly (W), and (h) northwesterly (NW), respectively. Black dots denote 25 weather stations of KMA and triangles denote 26 major thermoelectric power plants in South Korea (blue triangle < 1000 MW, red triangles ≥ 1000 MW).

Figure 13. Spatial distributions of temporal linear trends of (a) baseline ([$O_{3\,BL}$]), (b) seasonal component ([$O_{3\,SEASON}$]), and (c) long-term component ([$O_{3\,LT}$]) for the period 2000–2009 using data from 72 air quality monitoring sites of NIER.

Figure 14. The first leading mode of SVD between the long-term components of (a) daily maximum 8-h average O_3 ([$O_{3\,LT}$]) and (b) daily average NO_2 [$NO_{2\,LT}$] for the period 2000–

2009. (c) Spatial distribution of temporal linear trends of [$NO_{2\,LT}$]. (d) Time series of the SVD expansion coefficient associated with [$O_{3\,LT}$] mode (blue line) and [$NO_{2\,LT}$] mode (red line).

Table 1. 12-yr averaged concentrations and temporal linear trends of daily average O_3 ($O_{3\ avg}$) at 46 cities over South Korea for the period 1999–2010. The cities are categorized into three groups: 16 coastal cities, 14 inland cities, and 16 cities in the Seoul Metropolitan Area (SMA).

Coastal region	City code	$O_{3\ avg}$ (ppbv)	Trend (% yr^{-1})	Inland region	City code	$O_{3\ avg}$ (ppbv)	Trend (% yr^{-1})	SMA	City code	$O_{3\ avg}$ (ppbv)	Trend (% yr^{-1})
Busan*	BS	23.2	0.65	Andong	AD	22.0	1.35	Ansan	-	20.5	1.81
Changwon	CW	25.1	1.62	Cheonan	CN	18.7	0.72	Anyang	-	16.8	0.67
Gangneung	GN	26.5	2.61	Cheongju	CJ	21.0	1.25	Bucheon	-	18.3	1.71
Gimhae	-	24.4	-0.05	Daegu*	DG	19.8	0.77	Ganghwa	GH	30.9	1.12
Gunsan	GS	22.5	0.66	Daejeon*	DJ	20.7	1.21	Goyang	-	19.1	0.77
Gwangyang	-	28.1	-1.28	Gimcheon	-	24.4	2.36	Gunpo	-	19.6	-0.86
Jeju	JJ1	32.6	2.59	Gumi	GM	22.6	3.70	Guri	-	18.1	-0.83
Jinhae	-	31.3	1.03	Gwangju*	GJ	20.5	3.50	Gwacheon	-	17.6	-1.25
Masan	-	25.2	0.85	Gyeongju	-	22.1	-0.27	Gwangmyeong	-	18.0	0.41
Mokpo	MP	30.3	-0.21	Iksan	-	17.7	2.64	Incheon*	IC	19.0	1.45
Pohang	PH	25.7	0.01	Jecheon	JC	21.0	-0.21	Pyeongtaek	-	19.9	2.75
Seosan	SS	27.5	-1.67	Jeonju	JJ2	18.9	2.55	Seongnam	-	18.8	0.66
Suncheon	-	25.7	0.92	Jinju	JJ3	24.0	2.54	Seoul*	SU	17.1	2.82
Ulsan*	US	21.5	1.61	Wonju	WJ	20.7	-0.24	Siheung	-	21.0	2.29
Yeongam	-	28.6	3.58					Suwon	SW	19.3	1.86
Yeosu	YS	28.1	1.18					Uijeongbu	-	19.9	1.46
Coastal averages		26.6	0.88	Inland averages		21.0	1.56	SMA averages		19.6	1.05
Nationwide averages		22.5	1.15								

* : Major metropolitan cities in South Korea (Seoul, Busan, Daegu, Incheon, Gwangju, Daejeon, and Ulsan)

Table 2. Coefficients of determination (R^2) between baseline of daily maximum 8-h average O_3 ($O_{3\ 8h}$) and baselines of six meteorological variables (T_{max}, SI, TD, PS, WS, and RH) at 25 cities over South Korea for the period 1999–2010. Adjusted R^2 (*Adj.* R^2) between baseline of $O_{3\ 8h}$ and combined meteorological effects ($a_0 + \sum_i a_i\ MET_{BL}(t)_i$) are also represented. The cities are categorized into three groups: 10 coastal cities, 11 inland cities, and 4 cities in the Seoul Metropolitan Area (SMA). Numbers in bold fonts indicate correlations significant at the 95% level or higher.

	Cities	City code	Coefficients of determination (R^2)						*Adj.* R^2
			T_{max}	SI	TD	PS	WS	RH	MET_{BL}
Coastal region	Busan[1]	BS	0.147	**0.366**	0.139	**0.222**[2]	0.014	0.135	**0.408**
	Changwon	CW	**0.224**	n/a	**0.179**	**0.335**[2]	0.001[2]	**0.138**	**0.533**
	Gangneung	GN	0.013	**0.480**	0.000	0.072[2]	0.014	0.008[2]	**0.449**
	Gunsan	GS	0.032	n/a	0.017	0.047[2]	0.002	0.003[2]	0.164
	Jeju	JJ1	0.028[2]	0.080	0.069[2]	0.004	0.009	**0.141**[2]	**0.337**
	Mokpo	MP	0.012	**0.263**	0.004	0.038[2]	0.047[2]	0.043[2]	**0.427**
	Pohang	PH	0.034	**0.404**	0.014	0.102[2]	0.043[2]	0.003	**0.398**
	Seosan	SS	0.059	**0.495**	0.021	**0.135**[2]	0.001	0.049[2]	**0.506**
	Ulsan[1]	US	0.071	n/a	0.046	0.107[2]	0.035[2]	0.023	0.186
	Yeosu	YS	0.093	n/a	0.061	**0.140**[2]	0.002[2]	0.024	**0.251**
	Averages		0.071	0.348	0.055	0.120[2]	0.017	0.057	0.366
Inland region	Andong	AD	**0.269**	**0.544**	**0.128**	**0.379**[2]	0.004	0.026[2]	**0.628**
	Cheonan	CN	**0.400**	n/a	**0.263**	**0.479**[2]	0.003[2]	0.056[2]	**0.674**
	Cheongju	CJ	**0.387**	**0.666**	**0.219**	**0.443**[2]	0.052	0.053[2]	**0.674**
	Daegu[1]	DG	**0.381**	**0.621**	**0.224**	**0.493**[2]	0.002[2]	0.016	**0.703**
	Daejeon[1]	DJ	**0.312**	**0.721**	0.160	**0.408**[2]	0.089	0.062[2]	**0.724**
	Gumi	GM	**0.244**	n/a	0.116	**0.361**[2]	0.009[2]	0.038[2]	**0.563**
	Gwangju[1]	GJ	**0.274**	**0.502**	0.159	**0.315**[2]	0.015	0.005[2]	**0.570**
	Jecheon	JC	**0.258**	n/a	**0.137**	**0.365**[2]	0.012	0.108[2]	**0.589**
	Jeonju	JJ2	0.134	**0.434**	0.060	**0.179**[2]	0.008[2]	0.038[2]	**0.404**
	Jinju	JJ3	**0.199**	**0.413**	**0.129**	**0.238**[2]	0.000	0.012	**0.396**
	Wonju	WJ	**0.476**	**0.767**	**0.312**	**0.573**[2]	0.069	0.018[2]	**0.799**
	Averages		0.303	0.584	0.173	0.385[2]	0.024	0.039[2]	0.611
SMA	Ganghwa	GH	**0.204**	n/a	**0.158**	**0.274**[2]	**0.190**	0.025	**0.389**
	Incheon[1]	IC	**0.310**	**0.501**	**0.250**	**0.411**[2]	0.019[2]	0.097	**0.577**
	Seoul[1]	SU	**0.419**	**0.580**	**0.318**	**0.531**[2]	0.009[2]	0.045	**0.693**
	Suwon	SW	**0.525**	**0.703**	**0.422**	**0.640**[2]	0.009	0.080	**0.818**
	Averages		0.364	0.595	0.287	0.464[2]	0.057	0.062	0.619
Nationwide averages			0.220	0.502	0.144	0.292[2]	0.026	0.050[2]	0.514

[1] : Major metropolitan cities in South Korea

[2] : Negative correlation

n/a: Not available observations of SI

MET_{BL}: Combined meteorological variables regressed on $[O_{3\ BL}]$ ($a_0 + \sum_i a_i\ MET_{BL}(t)_i$)

Table 3. 12-yr averaged of daily minimum O_3 ($O_{3\ min}$) concentrations and daily average wind speeds (WS) at 46 cities over South Korea for the period 1999–2010. The cities are categorized into three groups: 16 coastal cities, 14 inland cities, and 16 cities in the Seoul Metropolitan Area (SMA).

Coastal region	City code	$O_{3\ min}$ (ppbv)	WS (m s^{-1})	Inland region	City code	$O_{3\ min}$ (ppbv)	WS (m s^{-1})	SMA	City code	$O_{3\ min}$ (ppbv)	WS (m s^{-1})
Busan*	BS	8.2	3.38	Andong	AD	5.6	1.61	Ansan	-	5.7	n/a
Changwon	CW	7.9	2.01	Cheonan	CN	4.9	1.79	Anyang	-	3.9	n/a
Gangneung	GN	11.1	2.86	Cheongju	CJ	6.0	1.70	Bucheon	-	5.9	n/a
Gimhae	-	7.7	n/a	Daegu*	DG	5.6	2.31	Ganghwa	GH	12.9	1.84
Gunsan	GS	8.8	3.07	Daejeon*	DJ	5.7	1.96	Goyang	-	6.2	n/a
Gwangyang	-	12.9	n/a	Gimcheon	-	7.9	n/a	Gunpo	-	4.8	n/a
Jeju	JJ1	15.4	3.31	Gumi	GM	7.1	1.53	Guri	-	4.4	n/a
Jinhae	-	13.3	n/a	Gwangju*	GJ	6.0	2.07	Gwacheon	-	4.8	n/a
Masan	-	8.6	n/a	Gyeongju	-	7.9	n/a	Gwangmyeong	-	5.6	n/a
Mokpo	MP	14.1	3.64	Iksan	-	6.4	n/a	Incheon*	IC	5.2	2.69
Pohang	PH	11.5	2.68	Jecheon	JC	6.1	1.51	Pyeongtaek	-	4.9	n/a
Seosan	SS	12.3	2.66	Jeonju	JJ2	6.5	2.02	Seongnam	-	5.8	n/a
Suncheon	-	9.4	1.16	Jinju	JJ3	8.2	1.37	Seoul*	SU	3.8	2.27
Ulsan*	US	7.5	2.12	Wonju	WJ	5.9	1.09	Siheung	-	6.6	n/a
Yeongam	-	13.7	n/a					Suwon	SW	5.2	1.86
Yeosu	YS	11.5	4.30					Uijeongbu	-	4.9	n/a
Coastal averages		10.9	2.84	Inland averages		6.4	1.72	SMA averages		5.6	2.17
Nationwide averages		7.7	2.26								

* : Major metropolitan cities in South Korea

n/a: Not available observations of wind speed

Table 4. Relative contributions (%) of short-term components ($[O_{3\ ST}]$), seasonal components ($[O_{3\ SEASON}]$), and long-term components ($[O_{3\ LT}]$) to total variance of log-transformed daily maximum 8-h average O_3 ($[O_3]$) at 25 cities over South Korea for the period 1999–2010. The cities are categorized into three groups: 10 coastal cities, 11 inland cities, and 4 cities in the Seoul Metropolitan Area (SMA).

Coastal region	City code	Relative contributions (%)			Inland region	City code	Relative contributions (%)			SMA	City cide	Relative contributions (%)		
		$[O_{3\ ST}]$	$[O_{3\ SEASON}]$	$[O_{3\ LT}]$			$[O_{3\ ST}]$	$[O_{3\ SEASON}]$	$[O_{3\ LT}]$			$[O_{3\ ST}]$	$[O_{3\ SEASON}]$	$[O_{3\ LT}]$
Busan*	BS	56.1	32.6	2.5	Andong	AD	32.7	53.2	3.6	Ganghwa	GH	56.2	33.1	3.2
Changwon	CW	53.6	36.2	2.0	Cheonan	CN	41.5	46.5	1.8	Incheon*	IC	58.7	32.7	1.5
Gangneung	GN	62.5	29.1	2.0	Cheongju	CJ	48.3	41.7	1.3	Seoul*	SU	51.8	38.2	3.8
Gunsan	GS	52.3	34.2	2.7	Daegu*	DG	50.4	41.3	1.6	Suwon	SW	42.0	49.4	1.8
Jeju	JJ1	53.8	29.2	4.3	Daejeon*	DJ	49.2	40.5	1.5					
Mokpo	MP	46.1	30.9	8.5	Gumi	GM	48.2	42.0	2.7					
Pohang	PH	53.9	34.4	4.1	Gwangju*	GJ	41.5	41.3	4.8					
Seosan	SS	45.1	35.6	5.3	Jecheon	JC	50.8	38.6	4.0					
Ulsan*	US	55.5	32.1	2.5	Jeonju	JJ2	47.4	36.1	4.2					
Yeosu	YS	52.2	34.1	4.3	Jinju	JJ3	55.5	29.2	6.2					
					Wonju	WJ	39.5	50.8	2.3					
Coastal averages		53.1	32.8	3.8	Inland averages		45.9	41.9	3.1	SMA averages		52.2	38.3	2.6
Nationwide averages		49.8	37.7	3.3										

* : Major metropolitan cities in South Korea

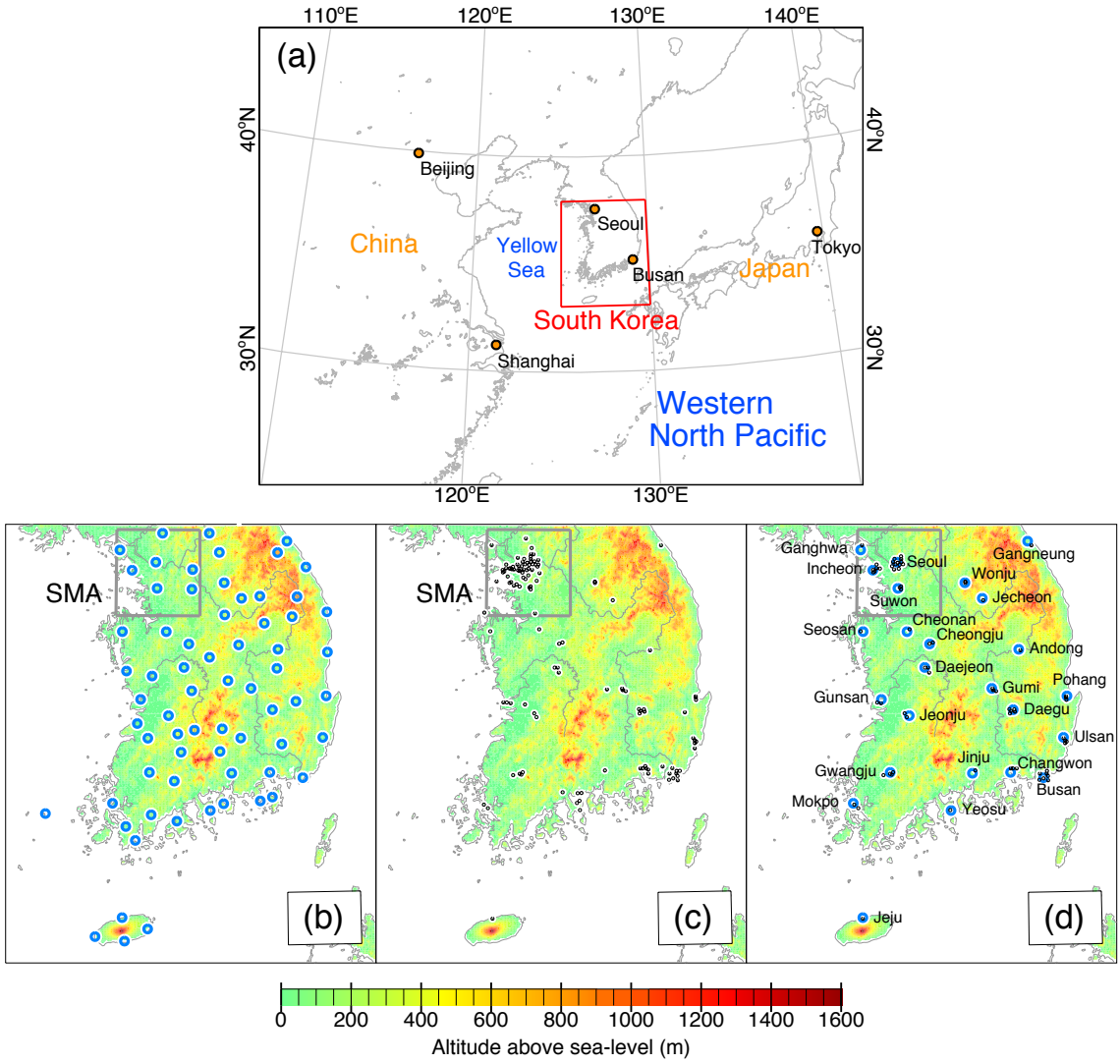

Figure 1. (a) Geographical locations of South Korea, and (b) 72 weather stations of the Korea Meteorological Administration (KMA) with blue circles, (c) 124 air quality monitoring sites of the National Institute of Environmental Research (NIER) with black dots, and (d) 72 air quality monitoring sites of NIER, which are located within 10 km from 25 weather stations of KMA over the South Korean domain.

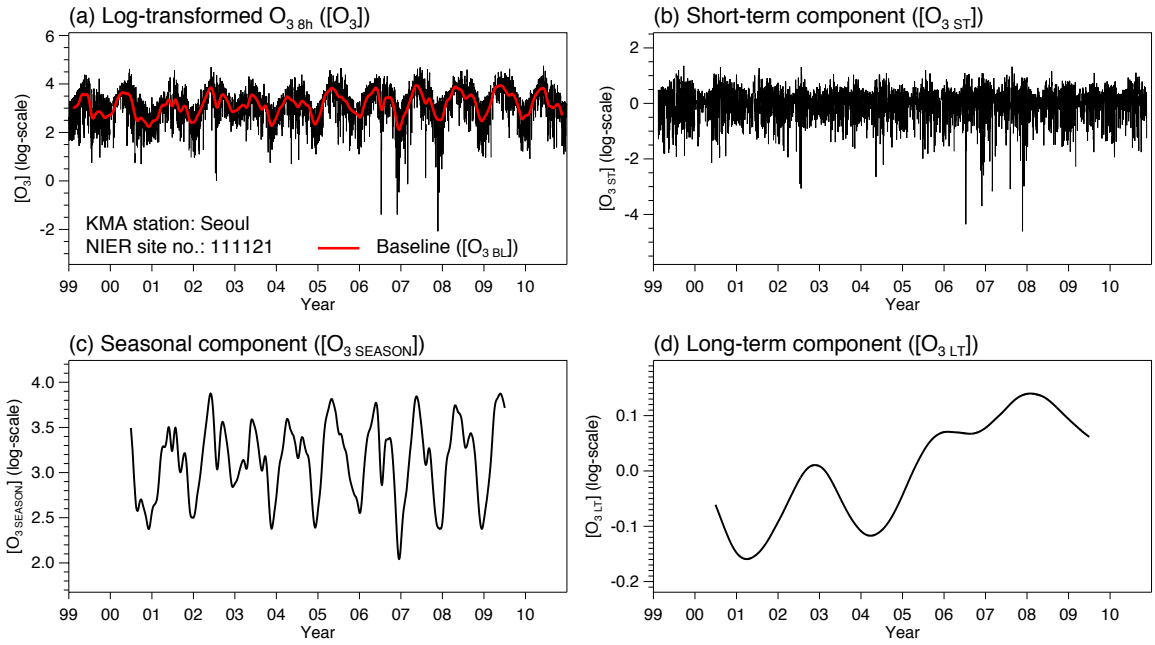

Figure 2. Time series of daily maximum 8-h average ozone ($O_{3\ 8h}$) at the City Hall of Seoul and its separated components such as (a) log-transformed $O_{3\ 8h}$ time series ([O_3]) and its baseline ([$O_{3\ BL}$]), (b) short-term component ([$O_{3\ ST}$]), (c) seasonal component ([$O_{3\ SEASON}$]), and (d) long-term component ([$O_{3\ LT}$]) by applying KZ-filter. It is noted that the longer window length causes the larger truncation of the result (Wise and Comrie, 2005) since the KZ-filter is an iterative moving average process. The baseline in red solid line is superimposed in (a).

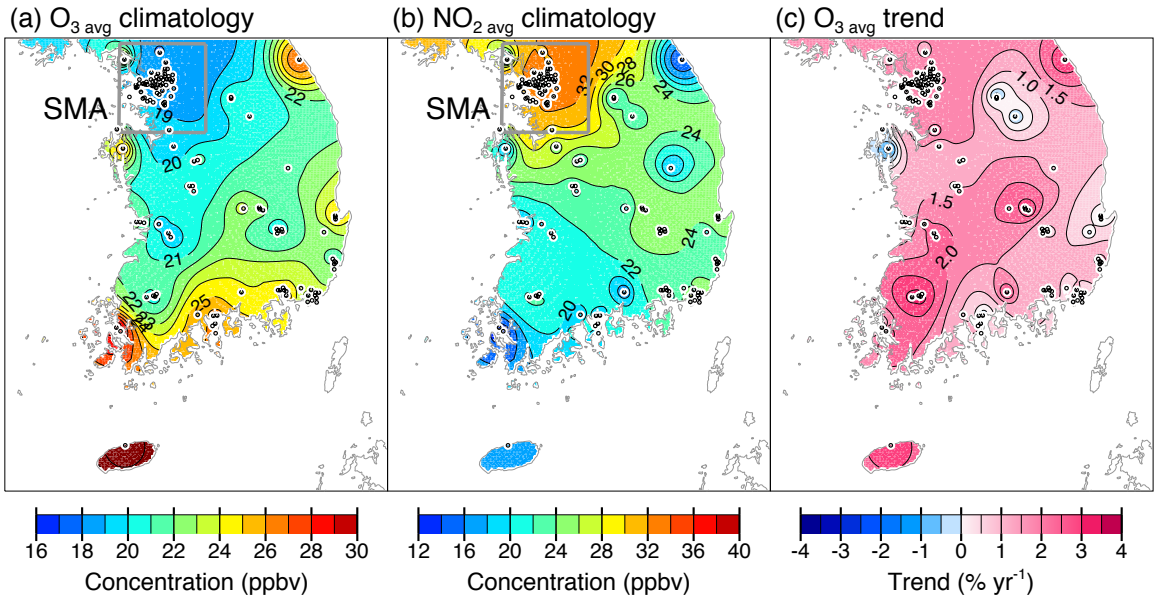

Figure 3. Spatial distributions of 12-yr averaged concentrations of (a) daily average O_3 ($O_{3\ avg}$) and (b) daily average nitrogen dioxide ($NO_{2\ avg}$), and (c) temporal linear trends of $O_{3\ avg}$ for the period 1999–2010 using data from 124 air quality monitoring sites (black dots) of NIER.

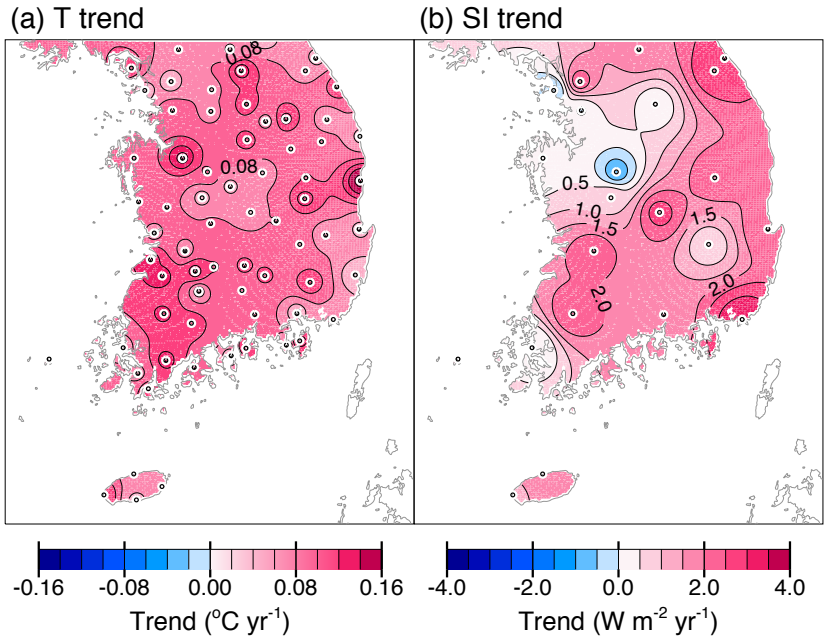

Figure 4. Spatial distributions of temporal linear trends of (a) daily average temperature (*T*) and (b) daily average surface insolation (SI) for the period 1999–2010 using data from 72 and 22 weather stations (black dots) of KMA, respectively.

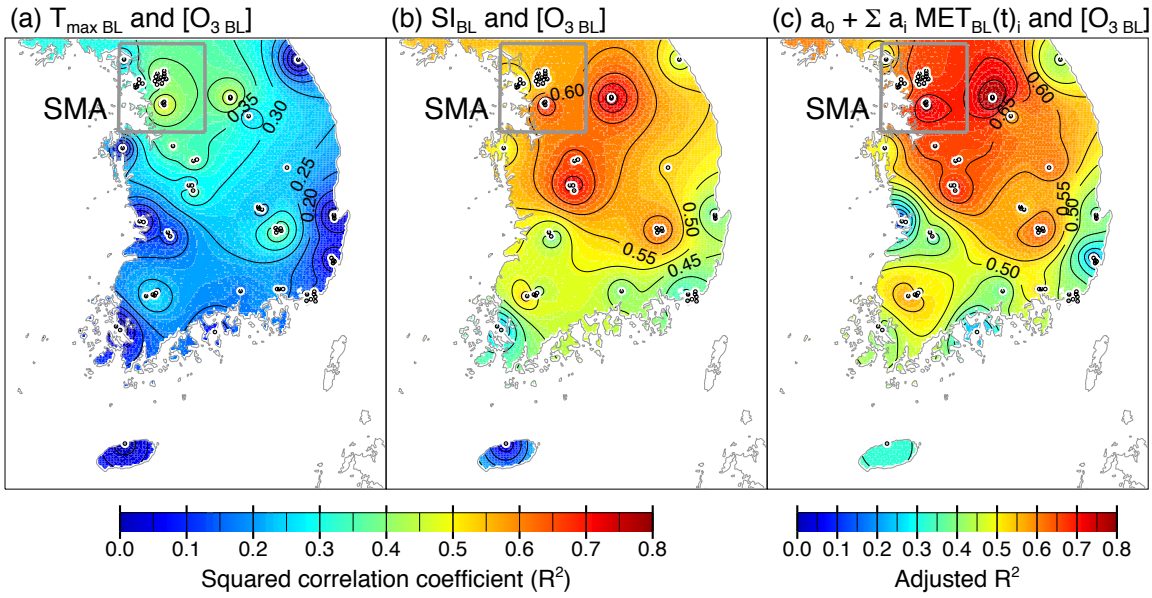

Figure 5. Spatial distributions of squared correlation coefficients (R^2) between baselines of $O_{3\ 8h}$ ($[O_{3\ BL}]$) and (a) daily maximum temperature ($T_{max\ BL}$) and (b) surface insolation ($SI_{\ BL}$). Black dots represent 72 air quality monitoring sites of NIER. (c) Spatial distribution of adjusted R^2 between $[O_{3\ BL}]$ and combined meteorological effects ($a_0 + \sum_i a_i\ MET_{BL}(t)_i$).

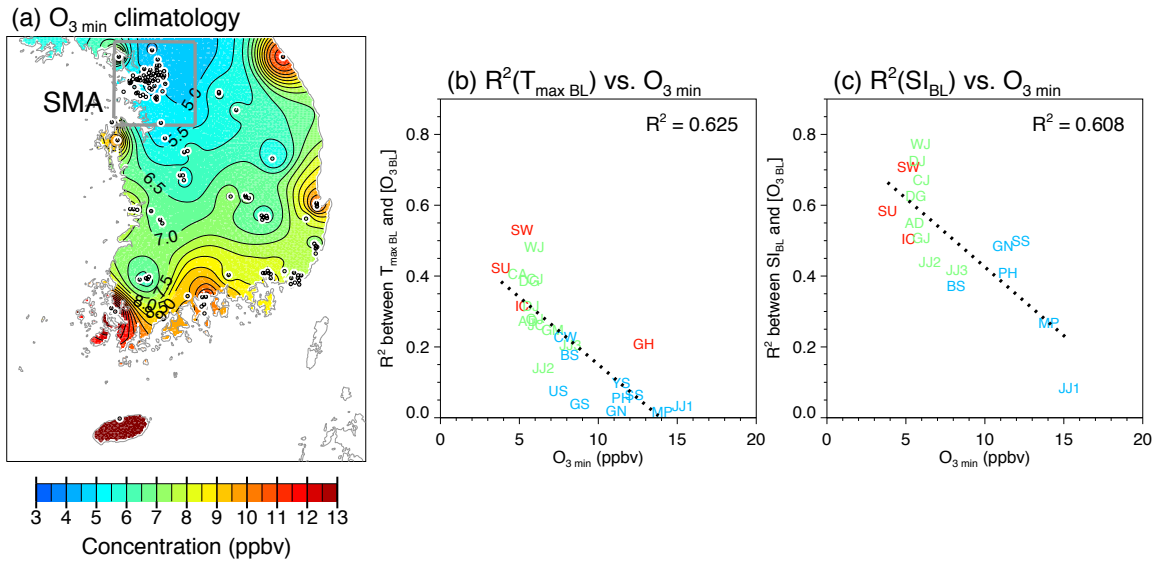

Figure 6. (a) Spatial distribution of 12-yr averaged concentrations of daily minimum O_3 ($O_{3\ min}$) for the period 1999–2010 using data from 124 air quality monitoring sites (black dots) of NIER. (b) Scatter plot of R^2 between [$O_{3\ BL}$] and $T_{max\ BL}$ versus $O_{3\ min}$ at 25 cities. (c) Scatter plot of R^2 between [$O_{3\ BL}$] and SI_{BL} versus $O_{3\ min}$ at 17 cities. City codes in red, green, and blue indicate the Seoul Metropolitan Area (SMA), inland, and coastal cities, respectively.

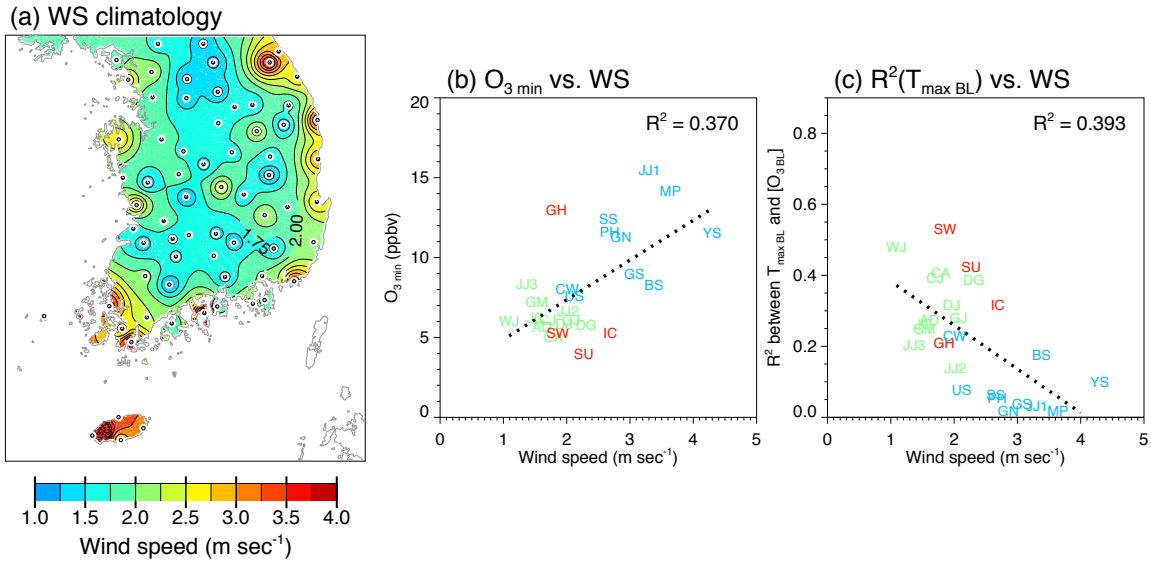

Figure 7. (a) Spatial distribution of 12-yr averaged daily average wind speeds (WS) for the period 1999–2010 using data from 72 weather stations (black dots) of KMA. (b) Scatter plot of $O_{3\ min}$ versus WS at 25 cities. (c) Scatter plot of R^2 between $[O_{3\ BL}]$ and $T_{max\ BL}$ versus WS at 25 cities. City codes in red, green, and blue indicate the Seoul Metropolitan Area (SMA), inland, and coastal cities, respectively.

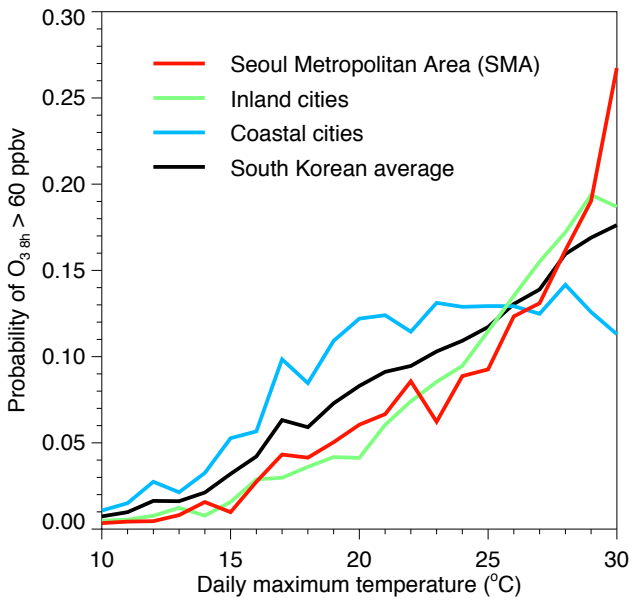

Figure 8. Probabilities of O_3 exceedances in the given range of daily maximum temperature (T_{max}) that $O_{3\ 8h}$ will exceed air quality standard of South Korea (60 ppbv).

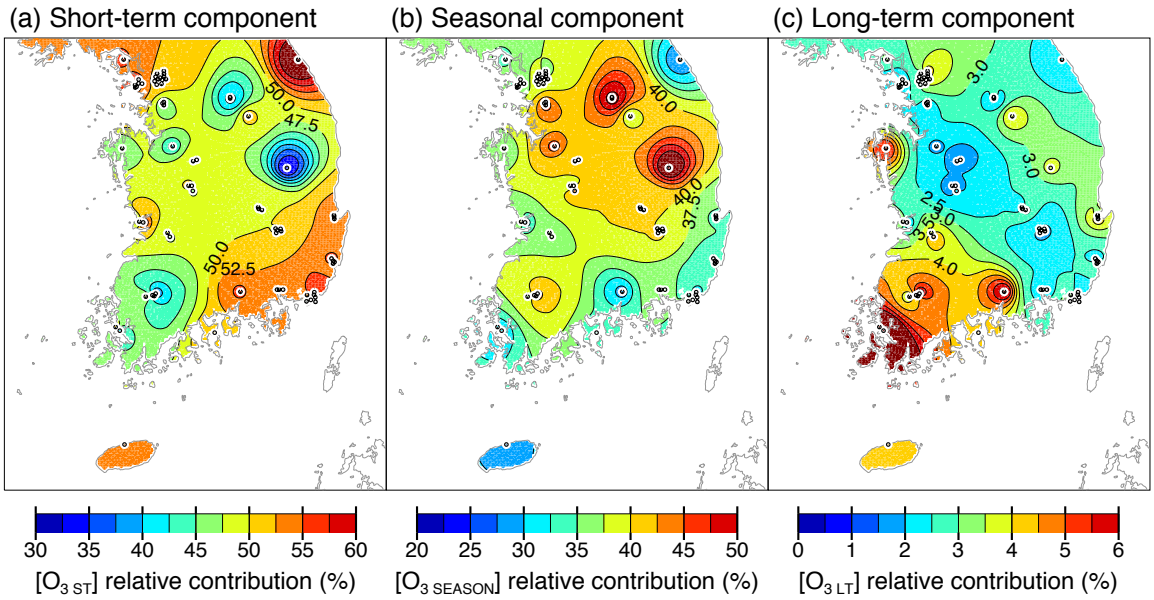

Figure 9. Spatial distributions of relative contributions of (a) short-term component ([$O_{3\ ST}$]), (b) seasonal component ([$O_{3\ SEASON}$]), and (c) long-term component ([$O_{3\ LT}$]) to the total variance of original time series ([O_3]) using data from 72 air quality monitoring sites (black dots) of NIER. Note that the color scales are all different.

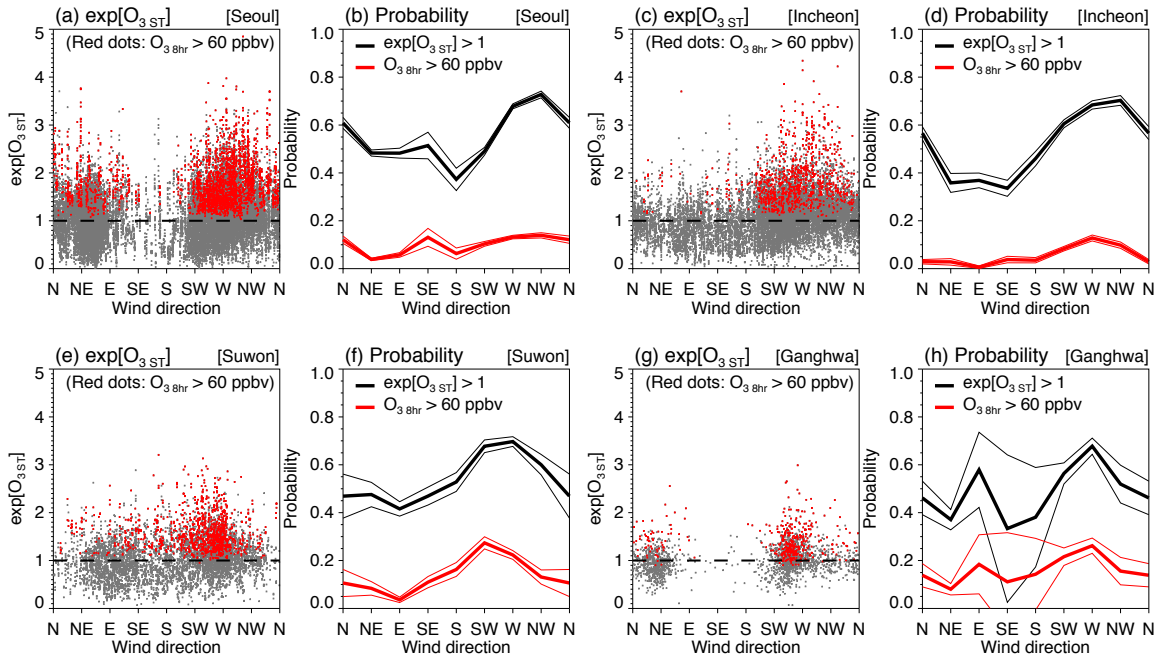

Figure 10. Relationships between wind directions (WD) and exponentials of short-term components ($\exp[O_{3\ ST}]$) during the months of frequent high O_3 events (May–October) at Seoul (a–b), Incheon (c–d), Suwon (e–f), and Ganghwa (g–h) in the Seoul Metropolitan Area (SMA) are represented in scatter plots of $\exp[O_{3\ ST}]$ versus WD (a, c, e, and g) and probabilities of O_3 exceedances in each WD (b, d, f, and h). Red dots in scatter plots denote high O_3 episodes that daily maximum 8-h average O_3 ($O_{3\ 8h}$) will exceed air quality standard of South Korea (60 ppbv). Dashed lines in scatter plots denote the reference of $\exp[O_{3\ ST}] = 1$. Probabilities of $\exp[O_{3\ ST}] > 1$ and $O_{3\ 8h} > 60$ ppbv in each WD are represented as black thick lines and red thick lines, respectively. 95% of confidence intervals for each probability are represented as black and red thin lines. We used O_3 data from 12 sites in Seoul, 6 sites in Incheon, 3 sites in Suwon, and 1 site in Ganghwa.

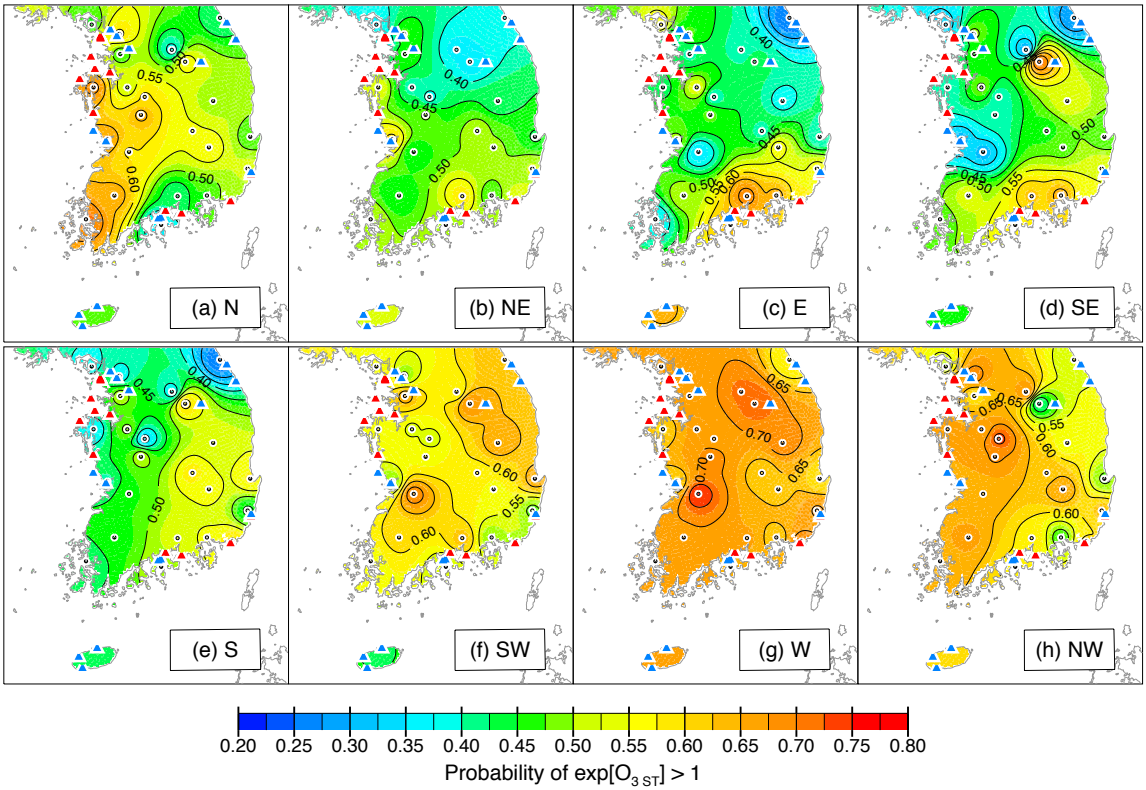

Figure 11. Spatial distributions of probabilities that exponentials of the short-term components will exceed 1 ($\exp[O_{3\ ST}] > 1$) for each wind direction (WD) of (a) northerly (N), (b) northeasterly (NE), (c) easterly (E), (d) southeasterly (SE), (e) southerly (S), (f) southwesterly (SW), (g) westerly (W), and (h) northwesterly (NW), respectively. Black dots denote 25 weather stations of KMA and triangles denote 26 major thermoelectric power plants in South Korea (blue triangle < 1000 MW, red triangles ≥ 1000 MW).

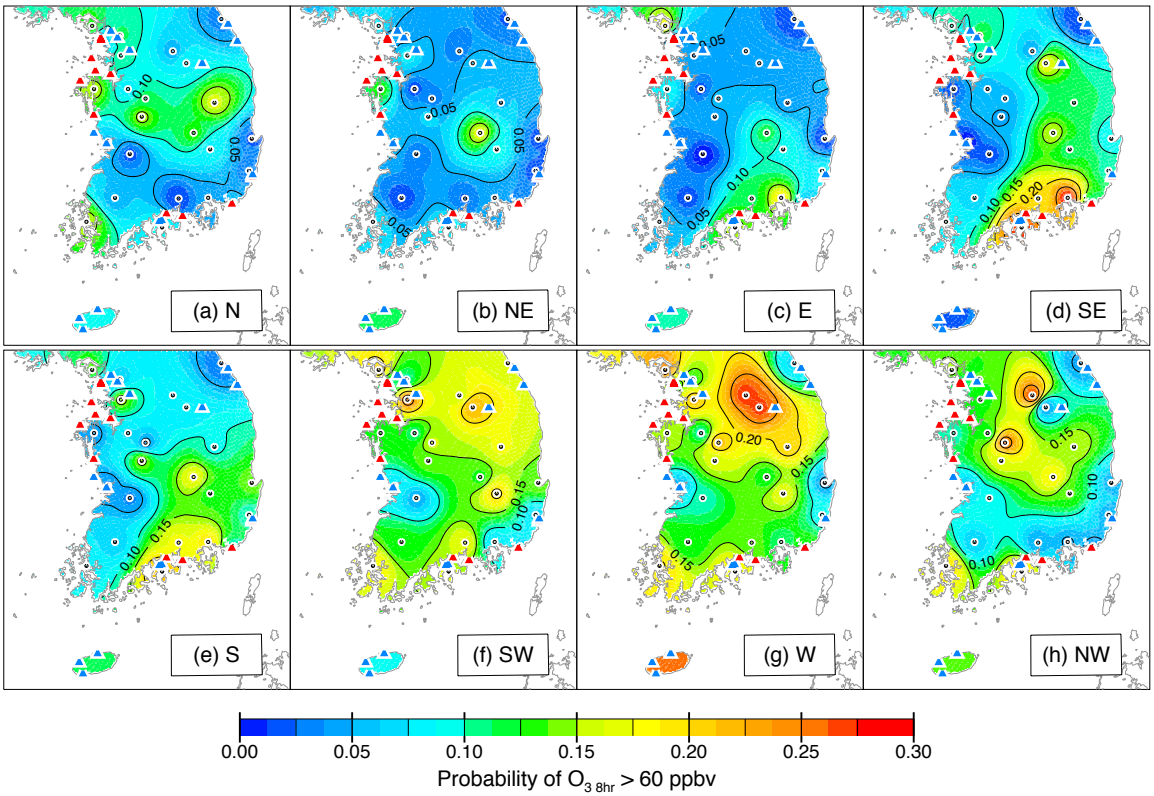

Figure 12. Spatial distributions of probabilities that daily maximum 8-h average O_3 ($O_{3\ 8h}$) will exceed air quality standard of South Korea (60 ppbv) for each wind direction (WD) of (a) northerly (N), (b) northeasterly (NE), (c) easterly (E), (d) southeasterly (SE), (e) southerly (S), (f) southwesterly (SW), (g) westerly (W), and (h) northwesterly (NW), respectively. Black dots denote 25 weather stations of KMA and triangles denote 26 major thermoelectric power plants in South Korea (blue triangle < 1000 MW, red triangles ≥ 1000 MW).

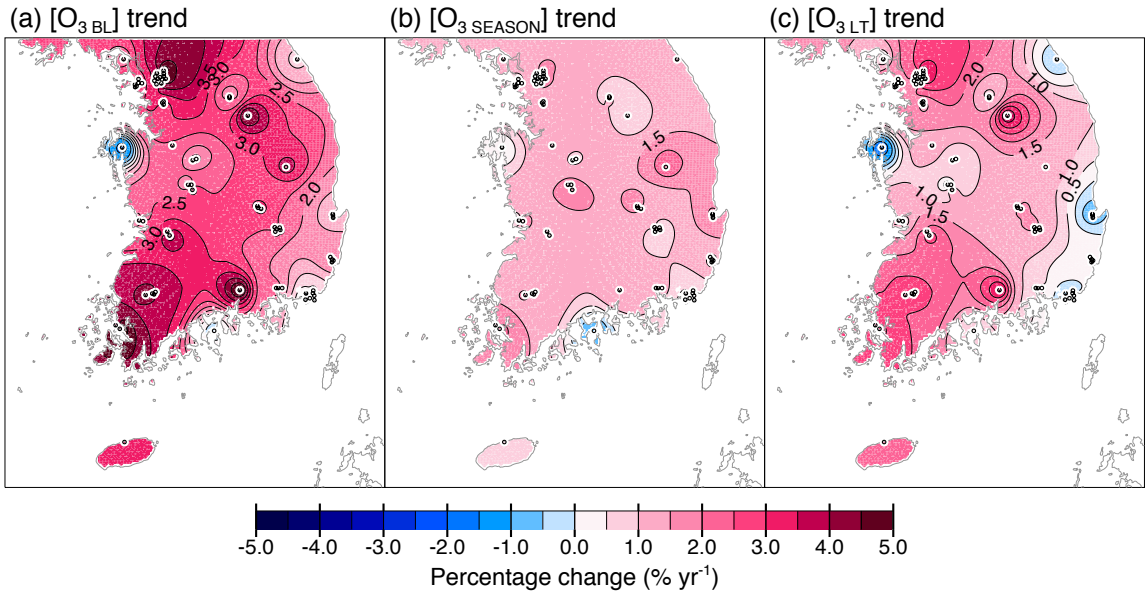

Figure 13. Spatial distributions of temporal linear trends of (a) baseline ([$O_{3\ BL}$]), (b) seasonal component ([$O_{3\ SEASON}$]), and (c) long-term component ([$O_{3\ LT}$]) for the period 2000–2009 using data from 72 air quality monitoring sites of NIER.

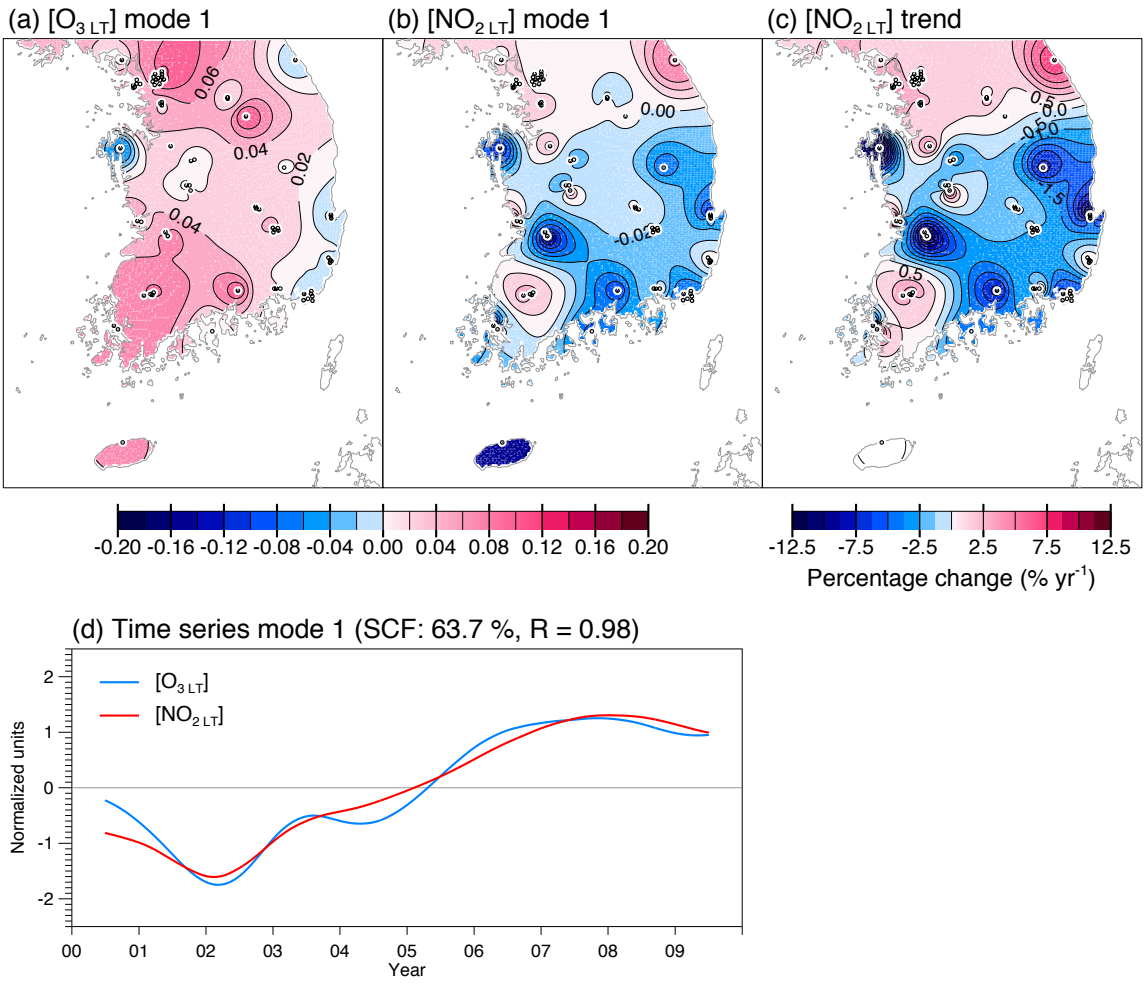

Figure 14. The first leading mode of SVD between the long-term components of (a) daily maximum 8-h average O_3 ([$O_{3\,LT}$]) and (b) daily average NO_2 [$NO_{2\,LT}$] for the period 2000–2009. (c) Spatial distribution of temporal linear trends of [$NO_{2\,LT}$]. (d) Time series of the SVD expansion coefficient associated with [$O_{3\,LT}$] mode (blue line) and [$NO_{2\,LT}$] mode (red line).